PAUL F. HOFFMAN SERIES

Evidence of Late Ediacaran Hyperextension of the Laurentian Iapetan Margin in the Birchy Complex, Baie Verte Peninsula, Northwest Newfoundland: Implications for the Opening of Iapetus, Formation of Peri-Laurentian Microcontinents and Taconic – Grampian Orogenesis

Cees R. van Staal[1], Dave M. Chew[2], Alexandre Zagorevski[3], Vicki McNicoll[3], James Hibbard[4], Tom Skulski[3], Sébastien Castonguay[5], Monica P. Escayola[6] and Paul J. Sylvester[7]

[1]Natural Resources Canada
Geological Survey of Canada
Vancouver, BC, Canada, V6B 5J3
E-mail: cvanstaa@nrcan.gc.ca

[2]Department of Geology
Trinity College Dublin
Dublin, Ireland

[3]Natural Resources Canada
Geological Survey of Canada
Ottawa, ON, Canada, K1A 0E8

[4]Department of Marine, Earth and Atmospheric Sciences
North Carolina State University
Raleigh, NC, USA, 27695-8208

[5]Natural Resources Canada
Geological Survey of Canada
Québec, QC, Canada, G1K 9A9

[6]CONICET
University of Buenos Aires
Buenos Aires, Argentina, C1428EHA

[7]Department of Earth Sciences
Memorial University
St. John's, NL, Canada, A1B 3X5

SUMMARY

The Birchy Complex of the Baie Verte Peninsula, northwestern Newfoundland, comprises an assemblage of mafic schist, ultramafic rocks, and metasedimentary rocks that are structurally sandwiched between overlying ca. 490 Ma ophiolite massifs of the Baie Verte oceanic tract and underlying metasedimentary rocks of the Fleur de Lys Supergroup of the Appalachian Humber margin. Birchy Complex gabbro yielded a Late Ediacaran U–Pb zircon ID–TIMS age of 558.3 ± 0.7 Ma, whereas gabbro and an intermediate tuffaceous schist yielded LA–ICPMS concordia zircon ages of 564 ± 7.5 Ma and 556 ± 4 Ma, respectively. These ages overlap the last phase of rift-related magmatism observed along the Humber margin of the northern Appalachians (565–550 Ma). The associated ultramafic rocks were exhumed by the Late Ediacaran and shed detritus into the interleaved sedimentary rocks. Psammite in the overlying Flat Point Formation yielded a detrital zircon population typical of the Laurentian Humber margin in the northern Appalachians. Age relationships and characteristics of the Birchy Complex and adjacent Rattling Brook Group suggest that the ultramafic rocks represent slices of continental lithospheric mantle exhumed onto the seafloor shortly before or coeval with magmatic accretion of mid-ocean ridge basalt-like mafic rocks. Hence, they represent the remnants of an ocean – continent transition zone formed during hyperextension of the Humber margin prior to establishment of a mid-ocean ridge farther outboard in the Iapetus Ocean. We propose that microcontinents such as Dashwoods and the Rattling Brook Group formed as a hanging wall block and an extensional crustal allochthon, respectively, analogous to the isolation of the Briançonnais block during the opening of the Alpine Ligurian–Piemonte and Valais oceanic seaways.

SOMMAIRE

Le complexe de Birchy de la péninsule de Baie Verte, dans le nord-ouest de Terre-Neuve, est constitué d'un assemblage de schistes mafiques, de roches ultramafiques et de métasédiments qui sont coincés entre des massifs ophiolitiques d'ascendance océanique de la Baie Verte au-dessus, et des métasédiments du Supergroupe de Fleur de Lys de la marge de Humber des Appalaches en-dessous. Le complexe de gabbro de Birchy a donné une datation U-Pb sur zircon ID-TIMS correspon-

Geoscience Canada, v. 40, http://dx.doi.org/10.12789/geocanj.2013.40.006 © 2013 GAC/AGC®

dant à la fin de l'Édiacarien, soit 558,3 ± 0,7 Ma, alors qu'un gabbro et un schiste tufacé intermédiaire montrent une datation LA-ICP-MS Concordia sur zircon de 564 ± 7,5 Ma et 556 ± 4 Ma, respectivement. Ces datations chevauchent la dernière phase de magmatisme de rift observée le long de la marge Humber des Appalaches du Nord (565-550 Ma). Les roches ultramafiques associées ont été exhumées vers la fin de l'Édiacarien et leurs débris ont été imbriqués dans des roches sédimentaires. Les psammites de la Formation de Flat Point susjacente ont donné une population de zircons détritiques typique de la marge laurentienne de Humber des Appalaches du Nord. Les relations chronologiques et les caractéristiques du complexe de Birchy et du groupe de Rattling Brook adjacent, permettent de penser que ces roches ultramafiques pourraient être des écailles de manteau lithosphérique continental qui auraient été exhumées sur le plancher océanique peu avant ou en même temps que l'accrétion magmatique de roches mafiques basaltiques de type dorsale médio-océanique. Par conséquent, elles seraient des vestiges d'une zone de transition océan-continent formée au cours de l'hyper-extension de la marge de Humber avant l'apparition d'une dorsale médio-océanique plus loin au large dans l'océan Iapétus. Nous proposons que des microcontinents comme de Dashwoods et du groupe de Rattling Brook ont constitués respectivement un bloc de toit et un allochtone crustal d'extension, de la même manière que le bloc Briançonnais a été isolé lors de l'ouverture des bras océaniques alpins de Ligurie-Piémont et de Valais.

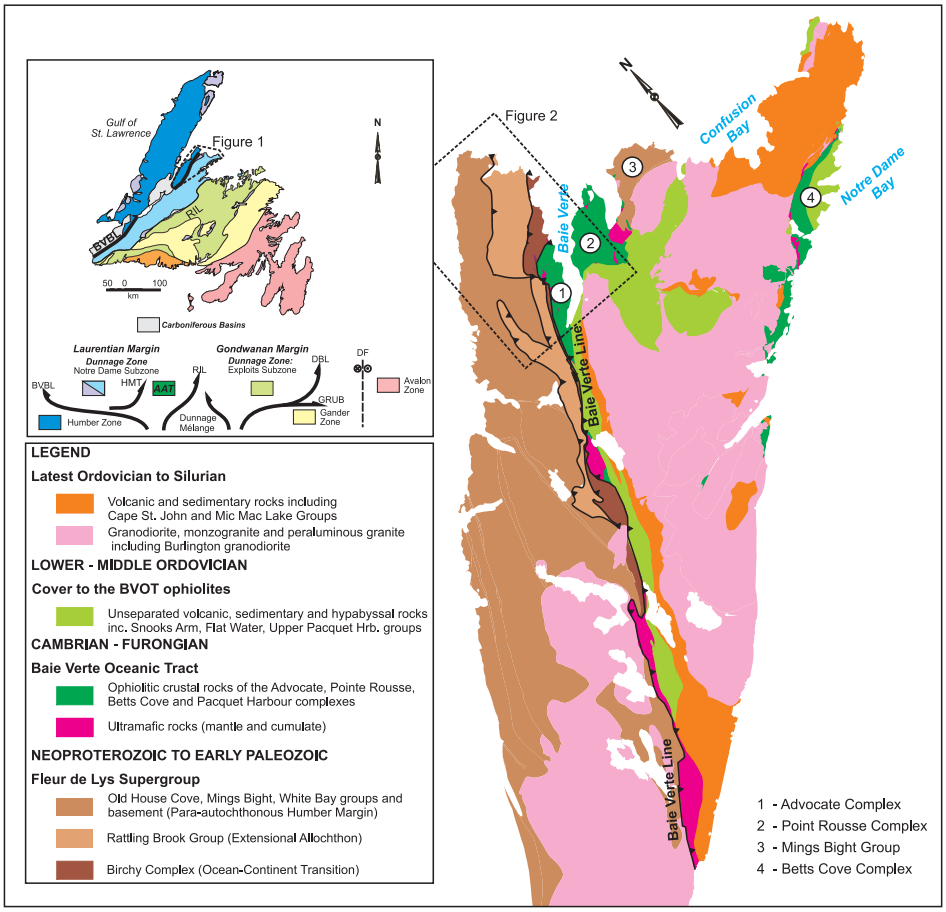

Figure 1. Simplified Geology of the Baie Verte Peninsula, northwestern Newfoundland (modified from Hibbard 1983 and Skulski et al. 2010). AAT: Annieopsquotch Accretionary Tract; BVBL: Baie Verte – Brompton Line; DBL: Dog Bay Line; DF: Dover Fault; GRUB: Gander River Untramafic Belt; HMT: Hungry Mountain Thrust; RIL: Red Indian Line.

INTRODUCTION

The timing and nature of the opening of the Iapetus Ocean along the Appalachian Humber margin of Laurentia (henceforth simplified to Humber margin) has been a contentious issue for a considerable time. In particular, breakup-related magmatism along the Humber margin spanned at least 200 my and appears to have involved several distinct pulses (Cawood et al. 2001; Tollo et al. 2004; Burton and Southworth 2010). The general consensus is that only the last major magmatic pulse between 615 and 550 Ma is related to opening of the Iapetus Ocean (Kamo et al. 1989; Cawood et al. 2001). This is consistent with the evidence for extensive Ediacaran normal faulting along the Humber margin (e.g. O'Brien and van der Pluijm 2012) and paleomagnetic evidence that suggests Late Ediacaran (ca. 570 Ma) separation of eastern Laurentia from its conjugate margin(s) (Cawood et al. 2001; McCausland et al. 2007). However, rift-related magmatism continued throughout the northern Appalachians for another 20 my (to ca. 550 Ma; Kumarapeli et al. 1989; Bédard and Stevenson 1999; Cawood et al. 2001; Hodych and Cox 2007; Burton and Southworth 2010, and references therein) and the thermal subsidence of Laurentia's (para)autochthonous rifted margin took place at least 40–50 my later (525–520 Ma; Bond et al. 1984; Williams and Hiscott 1987; Cawood et al. 2001; Waldron and van Staal 2001; Hibbard et al. 2007). The apparent conflict between paleomagnetic and geological data posed a major conundrum and called into question models of late Neoproterozoic opening of Iapetus.

In this contribution, we will discuss new ideas concerning the opening of Iapetus and the formation of peri-cratonic microcontinental blocks in light of our recent work on the Baie Verte Peninsula of northern Newfoundland (Figs. 1, 2). We will first present a brief overview of the previous models of opening of the Iapetus Ocean and then discuss pertinent geological data from the Fleur de Lys Supergroup, particularly the Birchy Complex on the Baie Verte Peninsula (Figs. 1, 2). The Birchy Complex has ophiolitic affinities (Bursnall 1975;

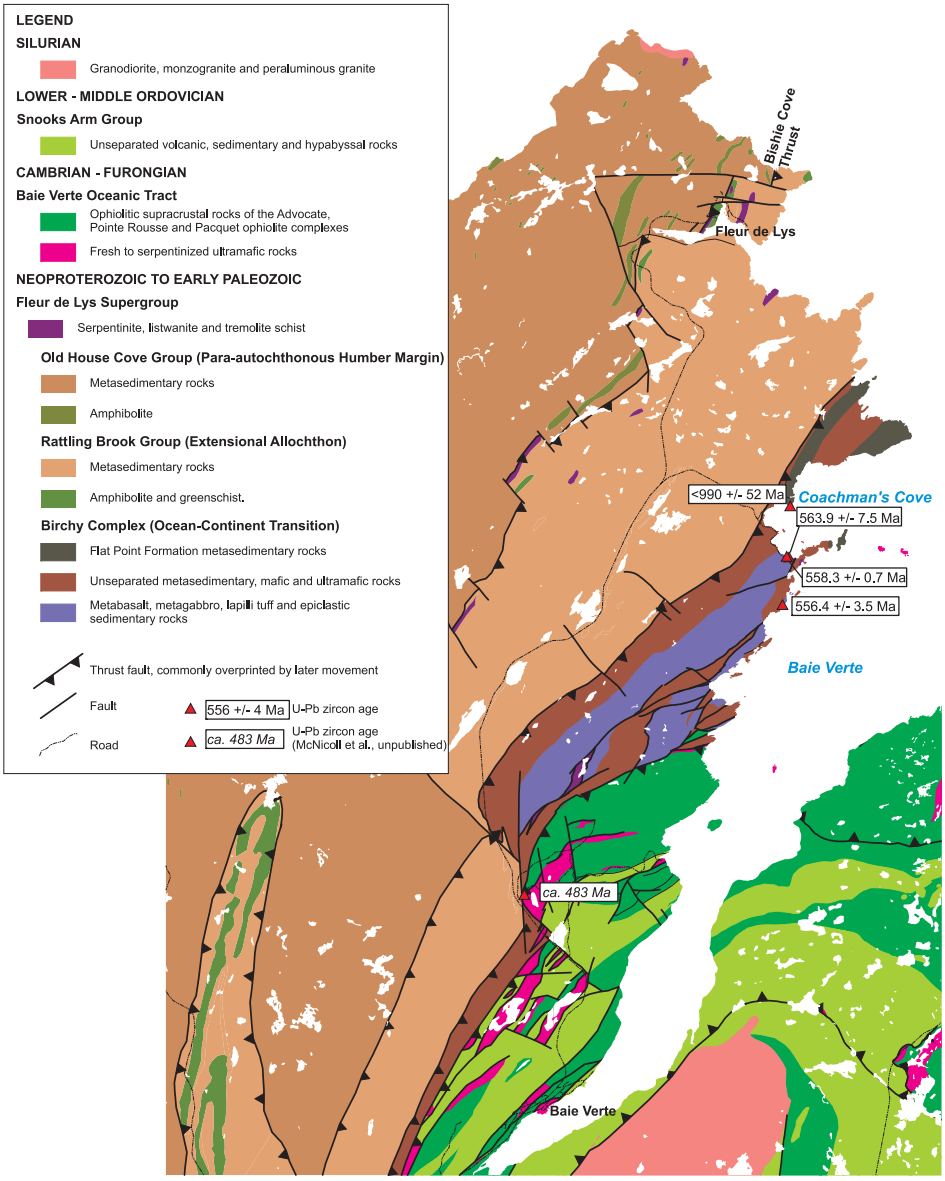

Figure 2. Geology of the main body of Birchy Complex and adjacent units near the town of Baie Verte. The ca. 483 Ma U–Pb zircon age date is from V. McNicoll, (pers. comm.).

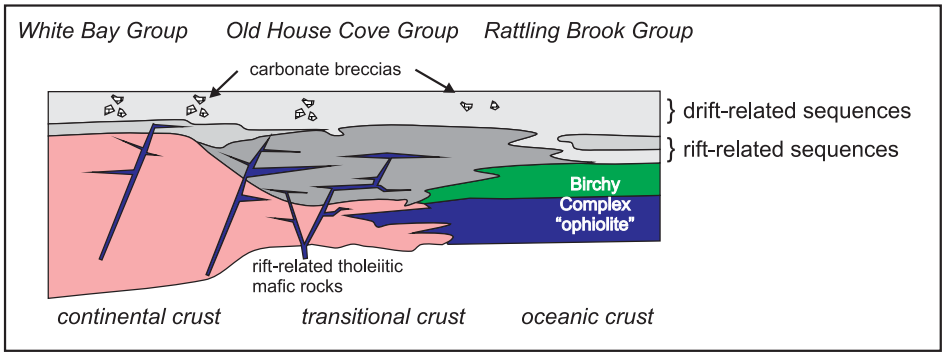

Figure 3. Schematic interpretation of the tectonic setting of units of the Fleur de Lys Supergroup in the Baie Verte Peninsula as proposed by Hibbard (1988), before the U–Pb zircon ages of the Birchy Complex were known.

Hibbard 1983), yet is closely associated and locally interleaved with clastic metasedimentary rocks typical of other units of the Ediacaran – Lower Ordovician Fleur de Lys Supergroup (Fig. 2), notably the Flat Point Formation (Kennedy 1971; Hibbard 1983). The Fleur de Lys Supergroup is generally considered to represent the more oceanward, distal remnant of the Laurentian Humber margin (Fig. 3), based on well-established lithological linkages (e.g. the presence of marble and marble breccia derived from the Humber platform) with the autochthonous, less deformed and metamorphosed parts of this margin (Bursnall and de Wit 1975; Williams 1977; Hibbard 1983; Hibbard et al. 1995; Cawood et al. 2001). We will mainly use new geochronological and geochemical data as evidence that the Birchy Complex and associated rocks of the adjacent Fleur de Lys Supergroup formed during hyperextension of the Humber margin in Newfoundland.

EXISTING MODELS CONCERNING THE TIME AND NATURE OF THE OPENING OF IAPETUS

Most modern models of the opening of the Iapetus Ocean are focussed on reconciling the discrepancy between the paleomagnetic and geological data. Typically, a two-stage rift-drift model is invoked. The first rift-drift event suggested by paleomagnetic data occurred between 590 and 570 Ma and resulted in the opening of Iapetus. The second break-up event, which led to the rift-drift transition on the Humber margin, between 540 and 530 Ma, was related to departure of a ribbon-shaped microcontinent, referred to as Dashwoods in the northern Appalachians (Cawood et al. 2001; Waldron and van Staal 2001; Allen et al. 2010). The separation of Dashwoods led to opening of the relatively narrow Taconic seaway (Hibbard et al. 2007; van Staal et al. 2007).

The 570–550 Ma magmatic rocks related to the second rift event generally range in composition from within-plate basalts to mid-ocean ridge basalt (MORB); the volcanic rocks are interleaved with continental margin-derived rift-stage clastic sediments (Bédard and Stevenson 1999; Hodych and Cox 2007). In addition, rift-related

magmatism included rhyolite, granite (Tollo et al. 2004) and tonalite (Cawood et al. 2001) along the length of the Northern Appalachians. This magmatism supports the existence of a latest Ediacaran and/or Early Cambrian rift-drift event. Other models call upon true polar wander to explain the apparent conflict between the paleomagnetic and geological datasets (Hodych and Cox 2007; Mitchell et al. 2011). This approach is anchored on the inference of a large, long-lived (615–550 Ma) mantle plume centred on southern Quebec (Puffer 2002). However, as pointed out by Burton and Southworth (2010), the broad age span and non-systematic geographical distribution of this phase of magmatism is not readily accommodated by the plume model.

The multiple rift model is viable, but is difficult to test and verify, because geological evidence for the first rift-drift event has not been identified. This rifting event should be recorded most extensively in the outboard Dashwoods ribbon (van Staal et al. 2007). However, with the exception of inherited Late Neoproterozoic zircons in Ordovician Notre Dame arc plutonic rocks (van Staal et al. 2007), evidence for such an event is completely masked by Early Paleozoic deformation, metamorphism and magmatism. In addition, the tectonic mechanism that caused the rifting-off of a continental ribbon like Dashwoods after Iapetus had already opened and was undergoing active spreading remains enigmatic. Potential mechanisms do exist, but generally involve ridge jumps and cessation of spreading along the old ridge (e.g. Yamasaki and Gernigon 2010), rather than the formation of two spreading centers that were active at the same time (cf. Burton and Southworth 2010). An alternative model involving protracted hyperextension of the Humber margin similar to the margins along the Alpine Tethys Ocean (Manatschal et al. 2006; Manatschal and Müntener 2009; Mohn et al. 2010) has not been previously explored but forms a viable solution to these seemingly conflicting datasets.

FLEUR DE LYS SUPERGROUP

The Fleur de Lys Supergroup comprises several groups of dominantly metaclastic psammitic and pelitic schist (see Figs. 1, 3), and some units dominated by mafic schist. These groups are generally considered, at least in part, to be coeval (Hibbard 1983; Hibbard et al. 1995), Ediacaran to Early Ordovician rocks deposited on or near the Humber margin (Fig. 3). The Rattling Brook Group and the Birchy Complex of the Fleur de Lys Supergroup were considered by Hibbard et al. (1995) to be the most oceanward (distal) remnants of the Humber margin. As both of these units contain ultramafic slivers, they are key to understanding the nature of the ocean – continent transition in the Iapetus Ocean.

The Birchy Complex

The Birchy Complex (Hibbard 1983) occurs in the immediate structural footwall of the ca. 490 Ma supra-subduction zone ophiolites (Figs. 1, 2; Hibbard 1983; Dunning and Krogh 1985; Cawood et al. 1996; Bédard et al. 2000; Skulski et al. 2010) of the Baie Verte oceanic tract (van Staal et al. 2007). The Birchy Complex comprises highly strained and metamorphosed polyphase-folded mafic schists (Fig. 4E, F) that are locally interlayered with psammite, graphitic pelite, calc-silicate, coticule, jasper and ultramafic rocks (Figs. 2, 4), and forms a steeply dipping, thin (ca. 1.0 – 2.5 km) structural unit.

The ultramafic rocks in the Birchy Complex vary from brecciated talc- and/or tremolite- bearing serpentinite, to listwanite (Fig. 4C) and bright green fuchsite – actinolite/tremolite schist. They principally occur as metre- to decimetre-scale lenses in highly deformed graphite-bearing mica schist and other metasedimentary rocks (Fig. 4B). Notably, prominent bodies of bright green fuchsite – actinolite/tremolite schist, which probably represent metamorphosed chromite-bearing pyroxenite and/or websterite bodies (see below), stand out and outline highly boudinaged and isoclinally folded horizons within the graphitic schist. Metasedimentary rocks locally contain detrital chromite, suggesting that they were in part derived from the ultramafic rocks. The protoliths of the mafic schists include metagabbro (Fig. 4B), lava, and pyroclastic and/or epiclastic rocks (Fig.4E; Hibbard 1983). No positive evidence for pillow structures has been identified, but the mafic schists locally include small lenses of jasper and epidosite (Fig. 4D) and are interlayered with coticule (Fig. 4F), suggesting that the schists represent highly deformed and metamorphosed submarine flows and/or high-level sills. Detailed structural mapping by Kennedy (1971), Bursnall (1975) and Hibbard (1983) indicates that the contact between the Birchy Complex and sedimentary rocks of the Fleur de Lys Supergroup (i.e. Flat Point Formation) is generally conformable and shows little or no evidence for accommodating enhanced shear strain (Figs. 2, 3).

Mafic and Ultramafic Rocks in the Rattling Brook Group

A narrow, discontinuous, linear belt of strongly metamorphosed Alpine-type ultramafic rocks (Bursnall 1975), interleaved with psammite and graphitic pelite and also associated with small lenses of amphibolite, occurs near the western boundary of the Rattling Brook Group in the northwestern part of the Baie Verte Peninsula (Fig. 2; Kennedy 1971; Hibbard 1983). These ultramafic rocks are associated with a major D_1 shear zone that was complexly refolded by tight to isoclinal F_2 folds (Kennedy 1971), which precludes kinematic analysis. This shear zone was previously referred to as the Bishie Cove slide (Fig. 2; Kennedy 1971), which we interpret as an early thrust that emplaced the Rattling Brook Group above correlative rocks in the Old House Cove Group (Figs. 2, 3; Kennedy 1971; Hibbard 1983). In addition to the presence of slivers of ultramafic tectonite, a thrust origin is consistent with the association of D_1 fabrics with local truncation of tectonostratigraphy in its footwall along strike (Hibbard 1983) and relatively high pressure (>10 kb) Taconic metamorphic assemblages (Kennedy 1971; Castonguay et al. 2010; Willner et al. 2012), suggesting that they formed during subduction. The ultramafic rocks adjacent to the Bishie Cove thrust commonly have been metamorphosed to soapstone, carbonate-bearing serpentinite and talc – tremolite – carbonate-bearing ultramafic schists. Graphitic schist hosts ultra-

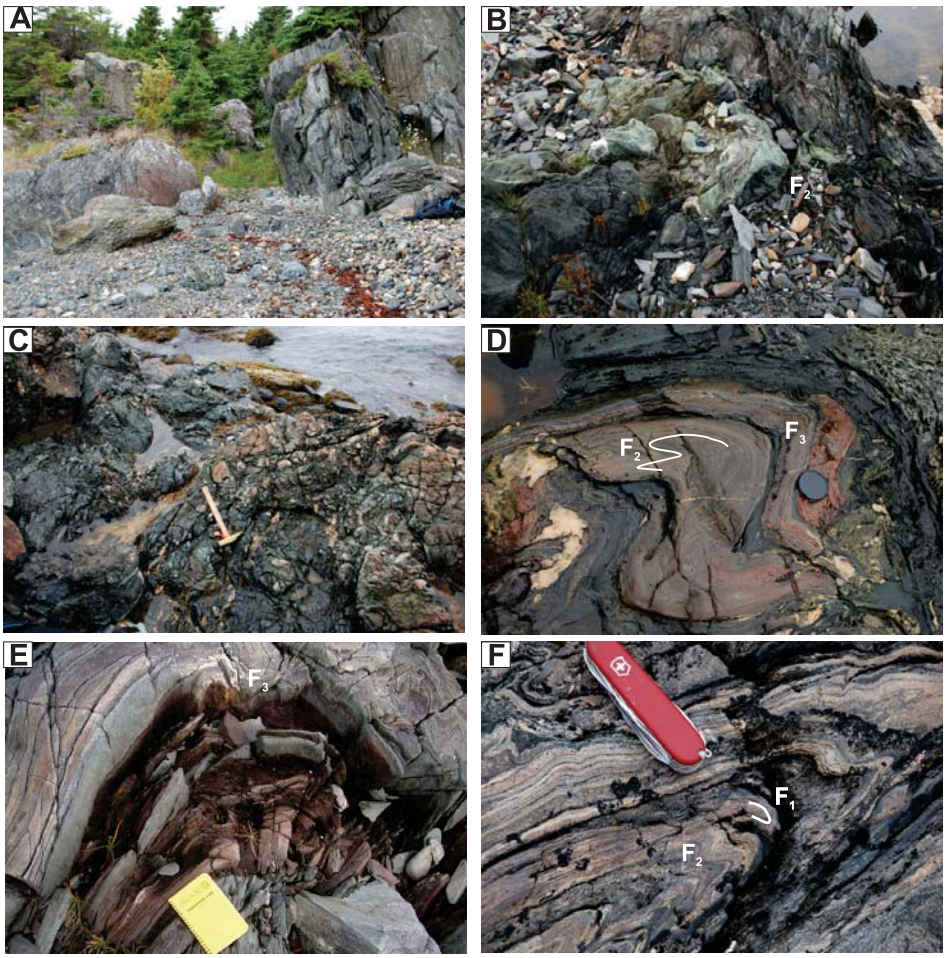

Figure 4. Representative photographs of the tectonites present in the Birchy Complex. A. Contact between mafic schist (right) and serpentinite (left) in Birchy Complex along shore east of Coachman's Cove. B. Slivers of tightly folded (F_2) actinolite/tremolite-fuchsite schist in broken-up dark metapelite and psammite. C. Brecciated serpentinite and listwanite. D. Complexly folded (F_2 and F_3) mafic schist with lenses of jasper and epidosite. E. F_3 fold in ca. 556 Ma intermediate tuff. F. Complexly folded (F_1 and F_2) coticule layers in mafic schist.

mafic rocks in both the Rattling Brook Group and Birchy Complex (Hibbard 1983), suggesting that they are correlative.

Existing Tectonic Interpretation of the Birchy Complex, Rattling Brook Group and Related Rocks

Correlatives of the Birchy Complex occur in the Mings Bight Group (e.g. Pelée Point schist; Fig. 1), which, like the Rattling Brook Group, is also dominated by meta-clastic rocks of the Fleur de Lys Supergroup (Hibbard 1983). The close spatial relationships between metasedimentary rocks of the Fleur de Lys Supergroup and ultramafic and mafic rocks of supposedly oceanic character in the Birchy Complex, the Mings Bight Group and Rattling Brook Group, led Hibbard (1988) to hypothesize that some of the sedimentary rocks in the Fleur de Lys Supergroups were deposited on oceanic lithosphere situated adjacent to the Humber margin; that is, the Fleur de Lys Supergroup overstepped the ocean – continent transition zone (Fig. 3). If a stratigraphic relationship between sedimentary rocks of the Fleur de Lys Supergroup (Flat Point Formation) and Birchy Complex is correct, the latter should represent ocean – continent transition lithosphere and/or juvenile oceanic lithosphere formed near this zone.

The contrasting association of ultramafic and sedimentary rocks and the highly dismembered tectonic character led to the suggestion that the Birchy Complex and correlatives represent zones of tectonic mélange that accommodated the initial stages of Early to Middle Ordovician obduction of the Baie Verte oceanic tract ophiolites onto the Humber margin (Bursnall 1975; Williams 1977; Hibbard et al. 1995). Although such a kinematic model is consistent with Middle Ordovician (Taconic, ca. 465 Ma) $^{40}Ar/^{39}Ar$ ages of muscovite and hornblende in the Birchy Complex mafic schists (van Staal et al. 2009a; Castonguay et al. 2010), metamorphic studies reveal that the Birchy Complex was buried to significantly greater depths (≥10 kb) during the Taconic than the structurally overlying Baie Verte oceanic tract (≤7 kb; Willner et al. 2012). Their present tectonic juxtaposition therefore took place subsequent to peak-Taconic burial metamorphism.

U–Pb ZIRCON AGES OF THE BIRCHY COMPLEX AND FLAT POINT FORMATION

To test Hibbard's (1988) hypothesis and constrain the age of the Birchy Complex, U–Pb geochronology of metagabbro and a tuffaceous schist of intermediate composition from the Birchy Complex were conducted by both the isotope dilution thermal ionization mass spectrometry (ID–TIMS) and laser-ablation inductively coupled plasma mass spectrometry (LA–ICPMS) techniques. Detrital zircon analyses from a Flat Point Formation psammite, sampled adjacent to the Birchy Complex on the shore of Coachman's Harbour (Fig. 2) were also undertaken by LA–ICPMS.

Analytical Methods

U–Pb ID–TIMS analyses were conducted at the Geochronology Laboratory at the Geological Survey of Canada, Ottawa. Heavy minerals were concentrated from the rock sample using standard crushing, grinding, and separation on a Wilfley table and by heavy liquid techniques. Mineral separates were sorted by magnetic susceptibility using a Frantz™ isodynamic separator and zircon grains were hand-picked and grouped on the basis of crystal morphology and quality using a binocular microscope. All zircon fractions analyzed were strongly air abraded

Table 1. U-Pb ID-TIMS analytical data.

Fraction[1]	Description[2]	Wt. ug	U ppm	Pb[3] ppm	$^{206}Pb/^{204}Pb$[4]	Pb[5] pg	Isotopic Ratios[6]								Ages (Ma)[8]					% Disc
							$^{208}Pb/^{206}Pb$	$^{207}Pb/^{235}U$	±1SE Abs	$^{206}Pb/^{238}U$	±1SE Abs	Corr.[7] Coeff.	$^{207}Pb/^{206}Pb$	±1SE Abs	$^{206}Pb/^{238}U$	±2SE	$^{207}Pb/^{235}U$	±2SE	$^{207}Pb/^{206}Pb$	±2SE	
SNB-06-017 (925): Birchy Complex metagabbro (UTM NAD83, zone 21, 563533E-5544585N)																				
A1 (Z; 14)	Co,Clr,Eu,El,fIn	22	43	4	459	11	0.20	0.73838	0.00391	0.09034	0.00012	0.556	0.05928	0.00028	557.5	1.4	561.5	4.6	577.4	20.3	3.6
A2 (Z; 14)	Co,Clr,Eu,El,fIn	31	46	5	4819	2	0.31	0.73466	0.00101	0.09047	0.00010	0.834	0.05889	0.00004	558.3	1.2	559.3	1.2	563.1	3.3	0.9
B1 (Z; 10)	Co,Clr,Tab,Frag,fIn	21	87	9	295	37	0.23	0.73623	0.00404	0.09031	0.00015	0.665	0.05913	0.00027	557.4	1.8	560.2	4.7	571.7	19.7	2.6
B2 (Z; 24)	Co,Clr,Tab,Frag,fIn	21	93	9	2420	4	0.20	0.73511	0.00157	0.09048	0.00016	0.917	0.05893	0.00005	558.4	1.9	559.5	1.8	564.4	3.8	1.1
C1 (Z; 15)	Co,Clr,Eu,Pr,fIn	22	120	12	2162	7	0.25	0.73410	0.00115	0.09034	0.00008	0.777	0.05893	0.00006	557.6	1.0	559.0	1.4	564.6	4.5	1.3
D1 (Z; 1)	pBr,Clr,Eu,Pr,fI	19	121	12	1026	13	0.21	0.73790	0.00184	0.09053	0.00010	0.597	0.05911	0.00012	558.7	1.1	561.2	2.2	571.2	8.9	2.3

Notes:

[1]Z=zircon. Number in bracket refers to the number of grains in the analysis. All zircon grains were physically air abraded.

[2]Fraction descriptions: Co=Colourless, pBr=pale brown, Clr=Clear, Eu=Euhedral, Pr=Prismatic, El=Elongate, Frag=Fragment, Tab=Tabular, fIn=Few Inclusions.

[3]Radiogenic Pb

[4]Measured ratio, corrected for spike and fractionation

[5]Total common Pb in analysis corrected for fractionation and spike

[6]Corrected for blank Pb and U and common Pb, errors quoted are 1 sigma absolute; procedural blank values for this study ranged from <0.1- 0.1 pg for U and 0.5-2 pg for Pb; Pb blank isotopic composition is based on the analysis of procedural blanks; corrections for common Pb were made using Stacey and Kramers (1975) compositions

[7]Correlation Coefficient

[8]Corrected for blank and common Pb, errors quoted are 2 sigma in Ma

(Krogh 1982). U–Pb ID–TIMS techniques utilized in this study are modified after Parrish et al. (1987), with treatment of analytical errors following Roddick (1987). U–Pb ID–TIMS analytical results are presented in Table 1 and displayed in a concordia plot (Figure 5A). The concordia diagram was produced and concordia age was calculated, with decay-constant errors included, using Isoplot v. 3.00 (Ludwig 2003).

Zircons for the LA–ICPMS analyses were separated from the crushed samples by conventional means at the Department of Geology, Trinity College Dublin, Ireland. The sub-300 μm fraction was processed using a Gemeni (Rogers) mineral separation table, and then the heavy fraction was passed through a Frantz magnetic separator at 1 A. The non-paramagnetic portion was then placed in a filter funnel with di-iodomethane and the resulting heavy fraction passed again through the Frantz magnetic separator at full current. All zircons were then hand picked in ethanol using a binocular microscope, mounted in a 25 mm epoxy resin disk, and polished to reveal their grain interiors. The mounts were gold-coated and imaged using an FEI Quanta 400 SEM equipped with a solid-state, twin-segment BSE detector at the Micro-Analysis Facility at Memorial University, Newfoundland (MUN). A cathodoluminescence probe was used to image internal structures, overgrowths and zonation (Fig. 6 A, B, C).

Isotopic data were obtained by LA–ICPMS at the MicroAnalysis Facility at Memorial University, Newfoundland and closely follow the procedures outlined in Pollock et al. (2009). Zircons were ablated *in situ* using a Lambda Physik COMPexPro 110 ArF excimer laser operating at a deep UV wavelength of 193 nm and a pulse width of 20 ns. A 10 μm laser beam was delivered to the sample surface and fired at a 10 Hz repetition rate using an energy density of 3 Jcm^{-2}. During ablation the sample was mounted in a sealed sample chamber and moved beneath the laser to produce a square 40 μm × 40 μm pit, to minimize the depth of ablation and reduce laser-induced elemental fractionation at the ablation site. The ablated sample was flushed from the sample cell and transported to the ICPMS system using a helium carrier gas (Q = 1.3 l/min), which reduces sample redeposition and elemental fractionation while increasing sensitivity for deep UV ablation. Mercury was filtered from the helium using gold-coated glass wool placed in the carrier gas line feeding the ablation cell. All analyses were performed by high-resolution ICPMS on a Finnigan Element XR system equipped with a dual-mode secondary electron multiplier operating in both counting and analogue modes. Data were collected using a 30 s measurement of the gas background before activation of the laser followed by 180 s of measurement with the laser on and zircon being ablated. The U and Pb isotopic ratios from the zircon were acquired along with a mixed ^{203}Tl–^{205}Tl–^{209}Bi–^{233}U–^{237}Np tracer solution (concentration of 10 ppb each) that was nebulized simultaneously with the ablated solid sample. Aspiration of the tracer solution allowed for a real-time instrument mass bias correction using the known isotopic ratios of the tracer solution measured while the sample was ablated; this technique is largely independent of matrix effects that can variably influence measured isotopic ratios and hence the resulting ages (Košler and Sylvester 2003).

Raw data for ^{207}Pb, ^{206}Pb, ^{204}Pb and ^{238}U were reduced using the macro-based spreadsheet program LAMDATE (Košler et al. 2008). The $^{207}Pb/^{206}Pb$, $^{206}Pb/^{238}U$ and $^{207}Pb/^{235}U$ ratios were calculated and blank corrected for each analysis. Laser-induced U/Pb fractionation was typically less than 0.05% per a.m.u. based on repeat measurements of the $^{206}Pb/^{238}U$ ratio of the reference standards. This fractionation was corrected using the intercept method of Sylvester and Ghaderi

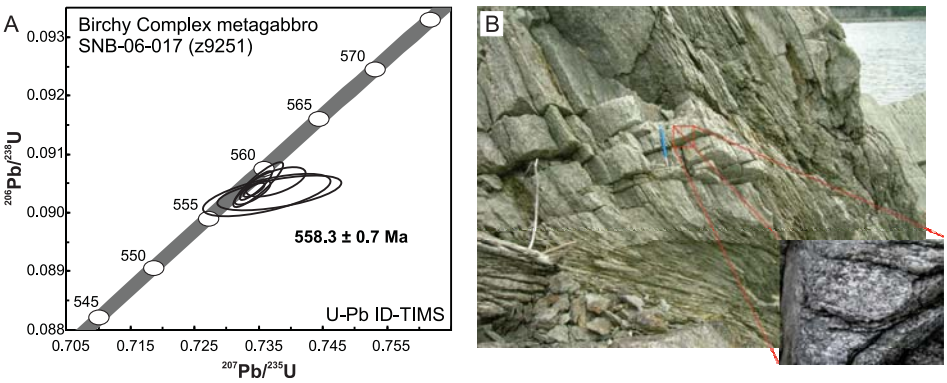

Figure 5. A. Concordia diagram with U–Pb ID–TIMS zircon analyses from the Birchy Complex metagabbro. B. Gabbro was sampled in a low strain pod where original igneous texture is locally preserved.

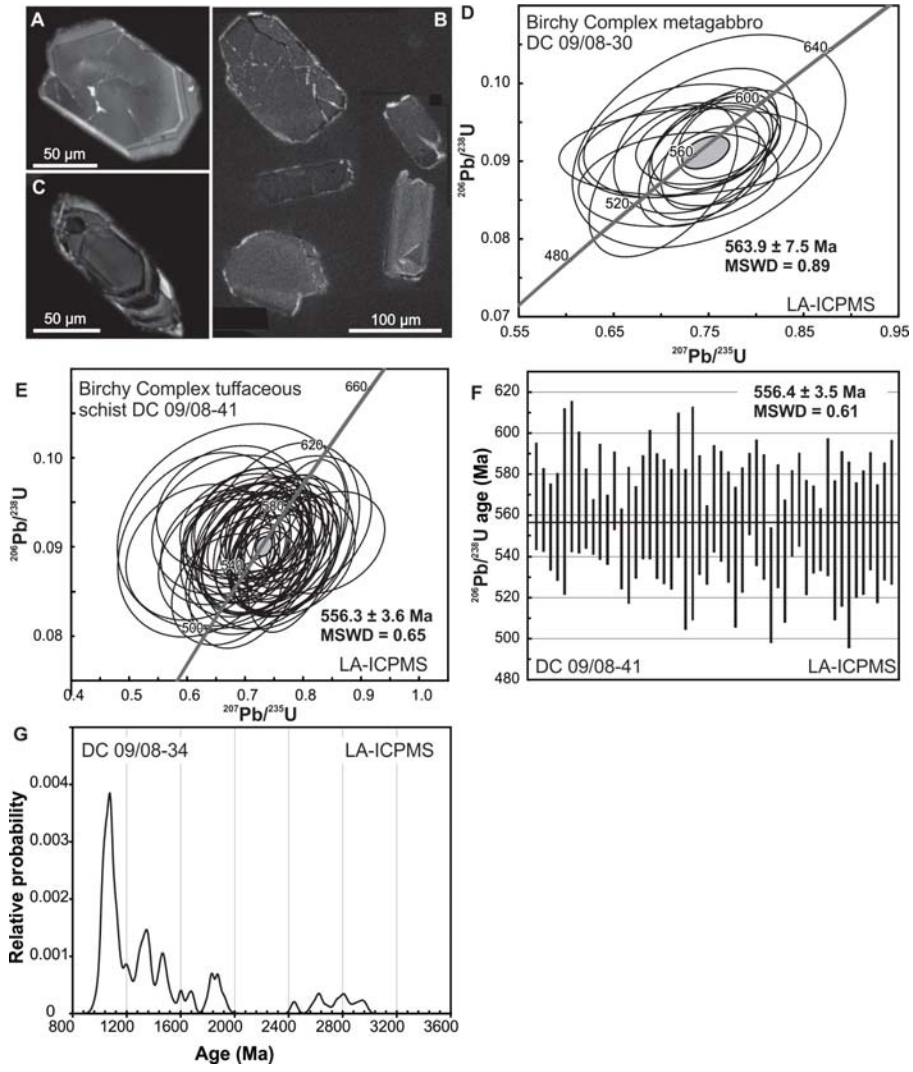

Figure 6. A. Representative cathodoluminescence image of a zircon grain from sample DC 09/08-30. B, C. Representative cathodoluminescence images of zircon grains from sample DC 09/08-41. D. Concordia diagram for metagabbro sample DC 09/08-30 (LA–ICPMS). E. Concordia diagram for tuffaceous intermediate schist sample DC 09/08-41 (LA–ICPMS, U–Pb zircon). F. Weighted mean of the $^{206}Pb/^{238}U$ ages for zircon from the tuffaceous schist (DC 09/08-41; LA–ICPMS). G. Relative probability plot for detrital zircon analyses in Flat Point Formation psammite (sample DC 09/08-34; LA–ICPMS).

(1997). For each analysis, time-resolved signals were inspected to ensure that only stable flat signal intervals were used in the age calculation. Measured $^{207}Pb/^{206}Pb$ ratios were not intercept-corrected; instead, the average ratio of the ablation interval selected for the age calculation was used. Analyses were rejected from the final dataset where the $^{207}Pb/^{206}Pb$ ratio calculated from the intercept-corrected $^{206}Pb/^{238}U$ and $^{207}Pb/^{235}U$ ratios did not fall within the 1σ uncertainty of the measured average $^{206}Pb/^{207}Pb$ ratio. Analyses that fell more than 5% above the $^{206}Pb/^{238}U$–$^{207}Pb/^{235}U$ concordia were also rejected. These two conservative filters ensured that any analyses that may have not been properly corrected for laser-induced U/Pb fractionation were eliminated from further consideration. High instrumental Hg backgrounds prohibited accurate measurement of ^{204}Pb. Thus, in the few analyses where ^{204}Pb was detected above background, the analysis was simply rejected from the dataset rather than attempting common Pb corrections.

Accuracy and reproducibility of U–Pb analyses in the MUN laboratory are routinely monitored by measurements of natural zircon standards of known U–Pb ID–TIMS age. To monitor the efficiency of mass bias and laser-induced fractionation corrections, standard reference materials 91500 zircon (1065 ± 3 Ma; Wiedenbeck et al. 1995) and Plešovice zircon (337.13 ± 0.37 Ma; Sláma et al. 2008) were analysed in this study before and after every eight unknowns. Age determinations were calculated using the U decay constants and the present-day $^{238}U/^{235}U$ ratio of 137.88 of Jaffey et al. (1971). Final ages and concordia diagrams were produced using the Isoplot/Ex macro (Ludwig 2003). Analytical data are listed in Table 2 and illustrated graphically in Fig. 6. The concordia ages for all analyses of 91500 and Plešovice zircon performed over the course of this study were 1066.7 ± 5.3 Ma (n = 77) and 337.7 ± 2.2 Ma (n = 52), respectively (95% confidence interval, with decay-constant errors included).

Birchy Complex Metagabbro

Metagabbro constitutes a significant component of the Birchy Complex

Table 2. LA-ICPMS U–Pb zircon data, samples DC 09/08-30, DC 09/08-34, DC 09/08-41.

	Measured Isotopic Ratios							Calculated Ages										Concentrations			
Analysis	$^{207}Pb/^{235}U$	1δ error	$^{206}Pb/^{238}U$	1δ error	Rho	$^{207}Pb/^{206}Pb$	1δ error	$^{207}Pb/^{235}U$ Ma	1δ error Ma	$^{206}Pb/^{238}U$ Ma	1δ error Ma	$^{207}Pb/^{206}Pb$ Ma	1δ error Ma	U-Pb/Pb-Pb concordancy	Concordia age (Ma)	2δ error Ma	MSWD (of concordance)	Probability	ppm ^{232}Th	ppm ^{238}U	Ratio Th/U
DC 09/08-30, metagabbro, Birchy Complex *[UTM 21U 0563584, 5544566]*																					
oc26a88	0.748647	0.025417	0.088479	0.002462	0.409866	0.058597	0.000756	567	15	547	15	552	28	99	557	24.74	1.71	0.19	64	137	0.464
oc26a89	0.747061	0.028765	0.089961	0.003417	0.493301	0.058748	0.000516	567	17	555	20	558	19	100	563	31.28	0.35	0.55	333	518	0.642
oc26a90	0.722130	0.042354	0.092620	0.002981	0.274352	0.058793	0.000758	552	25	571	18	559	28	102	566	32.01	0.53	0.47	148	156	0.949
oc26a91	0.761270	0.025046	0.091637	0.003198	0.530307	0.057499	0.000625	575	14	565	19	511	24	111	573	27.87	0.33	0.57	436	251	1.739
oc26a92	0.750346	0.058721	0.092571	0.005597	0.386319	0.058388	0.000667	568	34	571	33	544	25	105	570	55.80	0.00	0.95	346	327	1.058
oc26a93	0.746188	0.039254	0.092612	0.003807	0.390716	0.057472	0.000795	566	23	571	22	510	30	112	569	37.72	0.04	0.84	267	124	2.160
oc26a94	0.769699	0.021548	0.093183	0.002217	0.424851	0.058090	0.000467	580	12	574	13	533	18	108	577	21.45	0.15	0.70	432	326	1.327
no03a33	0.708233	0.038838	0.091211	0.002405	0.240458	0.060595	0.001036	544	23	563	14	625	37	90	559	26.44	0.63	0.43	151	208	0.726
no03a34	0.730589	0.056353	0.091209	0.002270	0.161360	0.066533	0.002190	557	33	563	13	823	69	68	562	26.03	0.03	0.86	221	95	2.317
no03a35	0.752095	0.025422	0.091738	0.002187	0.352569	0.059165	0.000609	569	15	566	13	573	22	99	567	22.55	0.05	0.82	439	221	1.983
no03a37	0.770513	0.034060	0.091706	0.003041	0.375096	0.060299	0.000992	580	20	566	18	614	36	92	572	31.06	0.47	0.49	383	234	1.635
no03a38	0.718128	0.042970	0.087660	0.002473	0.235722	0.063276	0.001269	550	25	542	15	718	43	75	543	27.68	0.09	0.76	332	233	1.424
no03a42	0.749213	0.030968	0.092239	0.002141	0.280766	0.061554	0.000671	568	18	569	13	659	23	86	568	23.13	0.00	0.96	291	341	0.854
no03a43	0.702248	0.031903	0.087600	0.004046	0.508338	0.056500	0.000405	540	19	541	24	472	16	115	540	36.12	0.00	0.96	1528	720	2.122
DC 09/08-34, psammite, Flat Point Formation, Rattling Brook Group *[UTM 21U 0563577 5545736]*																					
oc27a63	1.8249	0.0690	0.1781	0.0045	0.3331	0.0727	0.0009	1054	25	1056	25	1007	24	105	1055	40.25	0.01	0.94	35	76	0.469
oc27a64	2.8681	0.1608	0.2195	0.0074	0.3020	0.0934	0.0019	1374	42	1279	39	1496	39	86	1318	66.92	3.71	0.05	15	17	0.880
oc27a65	1.9069	0.0947	0.1852	0.0048	0.2613	0.0762	0.0012	1084	33	1095	26	1100	31	100	1091	45.75	0.10	0.75	24	44	0.554
oc27a66	3.3086	0.1230	0.2611	0.0081	0.4158	0.0928	0.0011	1483	29	1495	41	1483	22	101	1486	55.17	0.10	0.75	27	57	0.472
oc27a67	2.8646	0.1057	0.2351	0.0079	0.4547	0.0846	0.0007	1373	28	1361	41	1307	16	104	1371	53.99	0.09	0.76	27	113	0.240
oc27a68	16.5086	0.5497	0.5763	0.0184	0.4795	0.2069	0.0012	2907	32	2934	75	2881	9	102	2906	63.67	0.16	0.69	34	60	0.563
oc27a72	10.0423	0.2604	0.4261	0.0111	0.5036	0.1674	0.0007	2439	24	2288	50	2532	7	90	2440	47.81	12.28	0.00	66	142	0.463
oc27a74	3.6834	0.3414	0.2522	0.0169	0.3604	0.1120	0.0006	1568	74	1450	87	1832	9	79	1519	134.17	1.64	0.20	147	243	0.603
oc27a75	17.3807	0.4957	0.5695	0.0158	0.4867	0.2172	0.0013	2956	27	2906	65	2960	10	98	2958	54.53	0.78	0.38	32	39	0.810
oc27a76	2.0239	0.0876	0.1838	0.0052	0.3284	0.0805	0.0012	1124	29	1088	28	1209	29	90	1104	47.47	1.12	0.29	25	37	0.690
oc27a77	2.1843	0.1660	0.1832	0.0055	0.1976	0.0882	0.0024	1176	53	1085	30	1387	52	78	1100	56.77	2.57	0.11	23	42	0.548
oc27a81	1.7266	0.0684	0.1722	0.0042	0.3105	0.0735	0.0011	1019	25	1024	23	1027	29	100	1022	39.27	0.04	0.84	71	52	1.358
oc27a82	2.7844	0.0812	0.2344	0.0054	0.3971	0.0859	0.0008	1351	22	1357	28	1336	18	102	1353	40.37	0.05	0.83	27	63	0.422
oc27a83	5.0652	0.1031	0.3178	0.0070	0.5401	0.1113	0.0005	1830	17	1779	34	1821	7	98	1831	34.45	3.18	0.07	139	278	0.500
oc27a84	2.0908	0.1727	0.1742	0.0047	0.1645	0.0913	0.0034	1146	57	1035	26	1453	71	71	1047	50.28	3.30	0.07	44	67	0.658
oc27a85	1.7220	0.0451	0.1697	0.0034	0.3874	0.0737	0.0005	1017	17	1011	19	1033	14	98	1014	29.61	0.09	0.76	168	217	0.775
oc27a86	2.0756	0.0797	0.1939	0.0053	0.3547	0.0782	0.0007	1141	26	1143	29	1151	17	99	1142	44.97	0.00	0.96	73	137	0.532
oc27a90	2.2347	0.0832	0.2145	0.0049	0.3060	0.0757	0.0010	1192	26	1253	26	1087	26	115	1222	41.56	4.00	0.05	28	75	0.370
oc27a92	2.0400	0.0727	0.1835	0.0069	0.5293	0.0771	0.0005	1129	24	1086	38	1125	14	97	1124	48.28	1.78	0.18	33	193	0.171
oc27a93	1.9266	0.1093	0.1765	0.0058	0.2871	0.0803	0.0013	1090	38	1048	32	1203	33	87	1063	55.26	1.01	0.31	60	70	0.848
oc27a94	5.3691	0.1307	0.3267	0.0082	0.5126	0.1156	0.0006	1880	21	1822	40	1889	10	96	1879	41.68	2.88	0.09	55	152	0.365
oc27a95	2.0297	0.0654	0.1860	0.0055	0.4601	0.0774	0.0006	1126	22	1099	30	1132	15	97	1119	42.06	0.88	0.35	137	198	0.694
oc27a98	1.9040	0.1378	0.1737	0.0081	0.3204	0.0815	0.0019	1082	48	1033	44	1235	46	84	1053	75.62	0.84	0.36	77	85	0.905
oc27a99	14.1285	0.3531	0.5336	0.0108	0.4050	0.1903	0.0009	2758	24	2757	45	2745	8	100	2758	47.02	0.00	0.97	78	108	0.726
oc27a100	1.8703	0.0718	0.1823	0.0045	0.3201	0.0766	0.0010	1071	25	1079	24	1111	27	97	1075	40.38	0.09	0.76	47	78	0.596
oc27a101	3.8513	0.0779	0.2775	0.0056	0.4959	0.0982	0.0005	1604	16	1579	28	1590	10	99	1602	32.49	1.01	0.31	290	331	0.877
oc27a102	1.7739	0.1193	0.1794	0.0073	0.3016	0.0741	0.0015	1036	44	1063	40	1045	41	102	1051	66.65	0.31	0.58	17	26	0.664
oc27a103	3.6944	0.3558	0.2694	0.0186	0.3594	0.1027	0.0015	1570	77	1538	95	1673	27	92	1559	139.30	0.11	0.74	33	29	1.122
oc27a106	1.8018	0.0852	0.1659	0.0089	0.5689	0.0747	0.0007	1046	31	989	49	1059	19	93	1043	61.76	1.97	0.16	98	170	0.580
oc27a107	2.6861	0.1119	0.2127	0.0089	0.5010	0.0915	0.0008	1325	31	1243	47	1458	16	85	1313	61.25	3.88	0.05	192	223	0.863
oc27a108	1.9000	0.0970	0.1865	0.0064	0.3338	0.0747	0.0012	1081	34	1102	35	1062	31	104	1091	55.68	0.29	0.59	54	52	1.037
oc27a109	1.8825	0.0581	0.1810	0.0047	0.4213	0.0750	0.0005	1075	20	1072	26	1070	13	100	1074	37.82	0.01	0.91	42	278	0.150
oc27a110	5.6124	0.1537	0.3486	0.0079	0.4160	0.1144	0.0007	1918	24	1928	38	1870	12	103	1919	46.00	0.08	0.78	37	122	0.302
oc27a113	1.7986	0.0473	0.1762	0.0032	0.3459	0.0743	0.0005	1045	17	1046	18	1050	13	100	1046	28.50	0.00	0.95	127	274	0.462
oc27a114	13.0057	0.4670	0.4941	0.0159	0.4472	0.1899	0.0006	2680	34	2588	68	2741	5	94	2677	67.79	2.27	0.13	48	302	0.158
oc27a115	2.6462	0.0926	0.2283	0.0055	0.3434	0.0842	0.0010	1314	26	1326	29	1297	23	102	1319	44.36	0.15	0.70	24	79	0.300
oc27a116	1.7230	0.0358	0.1728	0.0031	0.4251	0.0721	0.0003	1017	13	1028	17	989	9	104	1020	24.67	0.41	0.52	258	781	0.331
oc27a118	2.6961	0.1001	0.2329	0.0060	0.3455	0.0862	0.0008	1327	27	1350	31	1343	18	100	1336	47.56	0.44	0.50	74	81	0.907
oc27a121	1.7534	0.0552	0.1750	0.0035	0.3201	0.0728	0.0007	1028	20	1040	19	1010	20	103	1035	32.17	0.24	0.62	150	118	1.269
oc27a122	2.7646	0.1367	0.2367	0.0045	0.1923	0.0929	0.0015	1346	37	1370	23	1487	31	92	1364	42.60	0.36	0.55	43	52	0.829
oc27a123	2.6198	0.1172	0.2182	0.0078	0.4003	0.0843	0.0013	1306	33	1272	41	1300	29	98	1295	60.78	0.68	0.41	39	35	1.134

(*continued*)

Table 2. (*Continued*) LA-ICPMS U–Pb zircon data, samples DC 09/08-30, DC 09/08-34, DC 09/08-41.

	Measured Isotopic Ratios							Calculated Ages										Concentrations			
Analysis	$^{207}Pb/^{235}U$	1δ error	$^{206}Pb/^{238}U$	1δ error	Rho	$^{207}Pb/^{206}Pb$	1δ error	$^{207}Pb/^{235}U$ Ma	1δ error Ma	$^{206}Pb/^{238}U$ Ma	1δ error Ma	$^{207}Pb/^{206}Pb$ Ma	1δ error Ma	U-Pb/Pb-Pb concordancy	Concordia age (Ma)	2δ error Ma	MSWD (of concordance)	Probability	ppm ^{232}Th	ppm ^{238}U	Ratio Th/U
DC 09/08-34, psammite, Flat Point Formation, Rattling Brook Group *[UTM 21U 0563577 5545736] (Continued)*																					
oc27a124	2.5822	0.0786	0.2195	0.0055	0.4097	0.0844	0.0006	1296	22	1279	29	1302	14	98	1291	41.56	0.34	0.56	78	189	0.412
oc27a125	1.8966	0.0656	0.1807	0.0043	0.3432	0.0761	0.0007	1080	23	1071	23	1098	18	98	1075	38.13	0.12	0.73	41	128	0.323
oc27a126	1.8027	0.0467	0.1714	0.0039	0.4346	0.0732	0.0007	1046	17	1020	21	1018	18	100	1038	31.58	1.64	0.20	259	181	1.433
oc27a129	1.8451	0.0562	0.1826	0.0038	0.3456	0.0746	0.0005	1062	20	1081	21	1057	14	102	1071	33.46	0.67	0.41	114	282	0.406
oc27a130	2.0553	0.0634	0.1884	0.0048	0.4115	0.0790	0.0004	1134	21	1113	26	1172	11	95	1127	38.73	0.67	0.41	199	589	0.338
oc27a131	1.5457	0.2101	0.1773	0.0100	0.2070	0.0720	0.0019	949	84	1052	55	986	55	107	1023	97.81	1.39	0.24	0	22	-0.021
oc27a132	2.1666	0.1084	0.1990	0.0056	0.2796	0.0830	0.0008	1170	35	1170	30	1270	19	92	1170	51.20	0.00	0.99	71	144	0.489
oc27a133	1.6923	0.0798	0.1629	0.0058	0.3767	0.0730	0.0012	1006	30	973	32	1013	34	96	990	51.82	0.89	0.35	69	36	1.917
oc27a134	11.7766	0.3566	0.4572	0.0133	0.4804	0.1832	0.0007	2587	28	2427	59	2682	6	91	2585	56.75	9.78	0.00	129	243	0.532
oc29a06	3.3084	0.1129	0.2512	0.0049	0.2879	0.0922	0.0011	1483	27	1445	25	1471	22	98	1462	42.06	1.51	0.22	150	121	1.235
oc29a07	5.6723	0.3871	0.3161	0.0176	0.4080	0.1330	0.0015	1927	59	1771	86	2137	20	83	1890	115.57	3.65	0.06	31	35	0.885
oc29a08	1.9222	0.0787	0.1842	0.0064	0.4227	0.0747	0.0006	1089	27	1090	35	1061	15	103	1089	50.74	0.00	0.98	28	218	0.130
oc29a09	15.2911	0.5641	0.5619	0.0191	0.4613	0.1948	0.0013	2834	35	2874	79	2783	11	103	2833	70.34	0.34	0.56	57	97	0.589
oc29a10	2.2006	0.1638	0.2000	0.0098	0.3289	0.0779	0.0014	1181	52	1175	53	1145	35	103	1178	85.34	0.01	0.92	18	41	0.446
oc29a21	1.8349	0.2275	0.1933	0.0093	0.1935	0.0725	0.0018	1058	82	1139	50	999	50	114	1119	90.97	0.91	0.34	10	23	0.416
oc29a22	2.4662	0.1225	0.2067	0.0095	0.4605	0.0883	0.0010	1262	36	1211	51	1390	21	87	1251	69.60	1.20	0.27	27	115	0.232
oc29a23	12.2608	0.2644	0.4763	0.0100	0.4859	0.1818	0.0008	2625	20	2511	44	2669	7	94	2626	40.45	9.01	0.00	90	221	0.406
oc29a24	1.9230	0.0998	0.1890	0.0058	0.2942	0.0749	0.0008	1089	35	1116	31	1066	21	105	1104	52.49	0.47	0.49	36	115	0.312
oc29a25	1.6827	0.1477	0.1691	0.0085	0.2862	0.0741	0.0015	1002	56	1007	47	1045	42	96	1005	81.11	0.01	0.93	14	28	0.486
oc29a26	14.8079	0.3653	0.5382	0.0148	0.5574	0.1931	0.0014	2803	23	2776	62	2769	12	100	2806	45.77	0.27	0.61	31	54	0.570
oc29a30	1.8261	0.1011	0.1792	0.0050	0.2513	0.0757	0.0011	1055	36	1062	27	1088	30	98	1060	48.40	0.04	0.85	35	62	0.562
oc29a31	3.1407	0.1021	0.2388	0.0063	0.4038	0.0940	0.0007	1443	25	1381	33	1508	14	92	1424	47.04	3.75	0.05	66	149	0.440
oc29a32	1.8222	0.1430	0.1754	0.0109	0.3970	0.0742	0.0014	1053	51	1042	60	1046	38	100	1049	92.16	0.04	0.85	28	33	0.851
oc29a33	5.1087	0.1123	0.3129	0.0067	0.4862	0.1151	0.0005	1838	19	1755	33	1882	8	93	1832	37.34	8.29	0.00	165	260	0.633
oc29a35	3.2374	0.1212	0.2538	0.0071	0.3734	0.0892	0.0010	1466	29	1458	36	1408	22	104	1463	52.93	0.05	0.82	44	62	0.709
oc29a40	2.8178	0.1091	0.2369	0.0073	0.3960	0.0873	0.0007	1360	29	1370	38	1366	15	100	1363	53.73	0.07	0.79	42	112	0.376
oc29a41	4.1211	0.1180	0.2924	0.0080	0.4756	0.1004	0.0006	1659	23	1654	40	1632	12	101	1658	46.41	0.02	0.89	193	157	1.227
oc29a43	1.8251	0.1001	0.1832	0.0069	0.3448	0.0749	0.0007	1055	36	1084	38	1066	18	102	1068	60.02	0.50	0.48	55	160	0.341
oc29a44	4.2698	0.1016	0.2912	0.0072	0.5215	0.1027	0.0008	1688	20	1648	36	1674	14	98	1687	39.15	1.69	0.19	61	103	0.588
oc29a49	2.6652	0.1246	0.2227	0.0098	0.4687	0.0848	0.0010	1319	35	1296	51	1310	23	99	1315	67.46	0.23	0.63	52	62	0.847
oc29a50	1.8438	0.0697	0.1808	0.0051	0.3708	0.0749	0.0007	1061	25	1071	28	1066	18	101	1065	43.18	0.12	0.73	67	183	0.367
oc29a51	5.3298	0.0958	0.3331	0.0056	0.4655	0.1125	0.0007	1874	15	1853	27	1840	12	101	1872	30.55	0.71	0.40	170	255	0.665
oc29a52	2.2739	0.1120	0.1962	0.0081	0.4170	0.0786	0.0009	1204	35	1155	43	1162	22	99	1188	64.59	1.32	0.25	95	224	0.422
oc29a53	2.2535	0.0572	0.1993	0.0054	0.5314	0.0799	0.0005	1198	18	1172	29	1194	12	98	1196	35.59	1.15	0.28	73	446	0.164
oc29a58	3.5144	0.1401	0.2523	0.0085	0.4244	0.1044	0.0004	1530	32	1451	44	1703	7	85	1511	60.72	3.66	0.06	201	539	0.373
oc29a59	1.9174	0.0347	0.1798	0.0028	0.4322	0.0771	0.0003	1087	12	1066	15	1123	9	95	1081	22.60	2.02	0.15	43	891	0.048
oc29a60	4.8510	0.1436	0.3267	0.0078	0.4041	0.1090	0.0008	1794	25	1822	38	1783	13	102	1799	47.88	0.62	0.43	131	120	1.094
oc29a61	2.4333	0.1563	0.2164	0.0082	0.2949	0.0830	0.0016	1252	46	1263	43	1270	38	99	1258	71.86	0.04	0.85	25	18	1.357
oc29a62	2.8265	0.0997	0.2326	0.0068	0.4158	0.0895	0.0008	1363	26	1348	36	1415	16	95	1359	49.94	0.18	0.67	111	175	0.633
oc29a66	3.2607	0.0979	0.2551	0.0064	0.4209	0.0926	0.0006	1472	23	1465	33	1480	12	99	1470	44.59	0.05	0.83	78	196	0.399
oc29a67	3.1044	0.1283	0.2553	0.0085	0.4015	0.0893	0.0009	1434	32	1466	44	1412	19	104	1442	59.49	0.57	0.45	23	65	0.354
DC 09/08-41, intermediate tuff, Birchy Complex *[UTM 21U 0563439 5543493]*																					
oc26a05	0.839068	0.041630	0.090498	0.002332	0.259680	0.064830	0.001206	619	23	558	14	769	39	73	569	26.20	6.28	0.01	32	46	0.684
oc26a07	0.743181	0.028960	0.091079	0.001849	0.260512	0.059968	0.001044	564	17	562	11	602	38	93	562	20.29	0.02	0.89	43	63	0.679
oc26a06	0.749850	0.027365	0.088876	0.001943	0.299477	0.059406	0.000763	568	16	549	12	582	28	94	554	21.08	1.33	0.25	135	123	1.100
oc26a14	0.767419	0.032971	0.088144	0.002407	0.317813	0.062152	0.001013	578	19	545	14	679	35	80	554	26.07	2.87	0.09	34	55	0.630
oc26a08	0.760799	0.055720	0.091238	0.004279	0.320149	0.059689	0.001394	574	32	563	25	592	51	95	567	45.45	0.12	0.73	25	41	0.614
oc26a09	0.789201	0.034594	0.090106	0.003948	0.499786	0.059080	0.000941	591	20	556	23	570	35	98	579	36.77	2.52	0.11	49	80	0.612
oc26a10	0.774941	0.031345	0.090921	0.002929	0.398260	0.058452	0.000740	583	18	561	17	547	28	103	571	29.58	1.24	0.27	90	125	0.725
oc26a13	0.726984	0.028370	0.091668	0.001784	0.249333	0.058351	0.000993	555	17	565	11	543	37	104	563	19.57	0.38	0.54	43	65	0.667
oc26a15	0.733357	0.016861	0.089459	0.001241	0.301566	0.059093	0.000557	559	10	552	7	571	21	97	554	13.34	0.35	0.55	211	233	0.903
oc26a16	0.716995	0.042725	0.092639	0.002556	0.231528	0.057619	0.000962	549	25	571	15	515	37	111	566	28.15	0.73	0.39	41	64	0.638
oc26a17	0.713625	0.023192	0.089874	0.001550	0.265346	0.059318	0.000577	547	14	555	9	579	21	96	553	16.91	0.30	0.58	184	258	0.712
oc26a18	0.777389	0.023014	0.091645	0.001819	0.335172	0.059508	0.000567	584	13	565	11	586	21	97	572	19.19	1.80	0.18	113	146	0.776
oc26a23	0.700425	0.020662	0.088515	0.001913	0.366297	0.057740	0.000425	539	12	547	11	520	16	105	543	19.46	0.33	0.56	531	380	1.399
oc26a24	0.702273	0.046426	0.089618	0.003040	0.256582	0.058450	0.001234	540	28	553	18	547	46	101	550	33.26	0.21	0.65	21	34	0.625

(*Continued*)

Table 2. *(Concluded)* LA-ICPMS U–Pb zircon data, samples DC 09/08-30, DC 09/08-34, DC 09/08-41.

	Measured Isotopic Ratios								Calculated Ages							Concentrations			
Analysis	$^{207}Pb/^{235}U$	1δ error	$^{206}Pb/^{238}U$	1δ error	Rho	$^{207}Pb/^{206}Pb$	1δ error	$^{207}Pb/^{235}U$ Ma	1δ error Ma	$^{206}Pb/^{238}U$ Ma	1δ error Ma	$^{207}Pb/^{206}Pb$ Ma	1δ error Ma	U-Pb/Pb-Pb concordancy	Concordia age (Ma)	2δ error Ma	MSWD (of concordance)	Probability (of concordance)	^{232}Th ppm	^{238}U ppm	Th/U Ratio
DC 09/08-41, intermediate tuff, Birchy Complex *[UTM 21U 0563439 5543493] (Concluded)*																					
oc26a25	0.675258	0.034851	0.090432	0.002014	0.215798	0.057422	0.001028	524	21	558	12	508	39	110	552	22.34	2.49	0.11	47	57	0.824
oc26a26	0.741030	0.030417	0.091461	0.002385	0.317586	0.057932	0.000821	563	18	564	14	527	31	107	564	25.17	0.00	0.95	44	67	0.652
oc26a27	0.671069	0.050595	0.094381	0.002849	0.200171	0.058588	0.001469	521	31	581	17	552	55	105	570	31.42	3.67	0.06	16	26	0.626
oc26a60	0.715514	0.047778	0.091133	0.002744	0.225458	0.058005	0.001275	548	28	562	16	530	48	106	560	30.48	0.24	0.63	39	46	0.847
oc26a32	0.780270	0.044683	0.088950	0.002723	0.267311	0.064275	0.001124	586	25	549	16	751	37	73	557	30.30	1.87	0.17	36	55	0.651
oc26a33	0.704265	0.037609	0.090375	0.002730	0.282857	0.059556	0.001031	541	22	558	16	587	38	95	553	29.29	0.49	0.49	40	60	0.670
oc26a34	0.791575	0.051608	0.092389	0.003199	0.265538	0.064599	0.001272	592	29	570	19	761	42	75	575	35.24	0.54	0.46	34	49	0.692
oc26a35	0.706621	0.042117	0.087966	0.003812	0.363516	0.055615	0.001073	543	25	543	23	437	43	124	543	39.12	0.00	0.98	34	51	0.664
oc26a40	0.679107	0.081440	0.092309	0.004708	0.212627	0.059660	0.002015	526	49	569	28	591	73	96	561	52.00	0.72	0.39	8	15	0.508
oc26a41	0.755696	0.032796	0.089547	0.002791	0.359072	0.059666	0.001010	572	19	553	17	591	37	93	560	29.07	0.85	0.36	56	68	0.835
oc26a42	0.731216	0.023199	0.087335	0.001794	0.323692	0.059941	0.000707	557	14	540	11	601	26	90	545	19.21	1.49	0.22	167	186	0.895
oc26a43	0.778008	0.035987	0.091200	0.002380	0.282121	0.062746	0.001030	584	21	563	14	700	35	80	568	26.03	1.02	0.31	78	64	1.227
oc26a44	0.699833	0.045824	0.092321	0.002405	0.198960	0.058927	0.001223	539	27	569	14	564	45	101	564	26.90	1.20	0.27	28	46	0.616
oc26a45	0.722453	0.031500	0.089960	0.002569	0.327442	0.058325	0.000983	552	19	555	15	542	37	102	554	26.95	0.03	0.87	44	62	0.712
oc26a50	0.620816	0.051593	0.089410	0.003106	0.208999	0.055382	0.001253	490	32	552	18	428	50	129	539	34.22	3.49	0.06	24	36	0.665
oc26a51	0.731366	0.043981	0.089277	0.002753	0.256370	0.060430	0.001303	557	26	551	16	619	47	89	553	30.40	0.05	0.82	19	35	0.541
oc26a52	0.771524	0.029189	0.091961	0.001820	0.261550	0.060074	0.000955	581	17	567	11	606	34	94	570	20.03	0.60	0.44	53	65	0.819
oc26a53	0.762097	0.036612	0.090949	0.002907	0.332619	0.058895	0.001006	575	21	561	17	563	37	100	566	30.68	0.39	0.53	59	56	1.060
oc26a54	0.770081	0.038046	0.089085	0.002831	0.321581	0.060267	0.001083	580	22	550	17	613	39	90	559	30.47	1.67	0.20	69	68	1.020
oc26a55	0.669276	0.039172	0.085227	0.002542	0.254837	0.059681	0.000918	520	24	527	15	592	33	89	526	28.09	0.08	0.78	41	93	0.437
oc26a59	0.701888	0.044106	0.090499	0.002724	0.239506	0.056887	0.001321	540	26	558	16	487	51	115	554	29.99	0.47	0.50	31	39	0.785
oc26a61	0.703381	0.043312	0.086791	0.002695	0.252113	0.059979	0.001294	541	26	537	16	603	47	89	537	29.91	0.03	0.87	23	54	0.432
oc26a62	0.696463	0.041980	0.091424	0.001842	0.167119	0.059766	0.001374	537	25	564	11	595	50	95	561	20.96	1.15	0.28	39	62	0.632
oc26a63	0.769094	0.030857	0.091282	0.002104	0.287301	0.059292	0.000904	579	18	563	12	578	33	97	567	22.88	0.75	0.38	68	102	0.661
oc26a64	0.718902	0.042114	0.088834	0.002514	0.241542	0.059467	0.001142	550	25	549	15	584	42	94	549	27.94	0.00	0.96	75	70	1.068
oc26a68	0.707118	0.029444	0.090099	0.001946	0.259408	0.057766	0.000758	543	18	556	12	521	29	107	553	21.24	0.52	0.47	68	90	0.750
oc26a69	0.717865	0.016995	0.088569	0.001450	0.345783	0.057558	0.000465	549	10	547	9	513	18	107	548	15.10	0.05	0.83	444	348	1.277
oc26a70	0.776971	0.044480	0.090183	0.003074	0.297659	0.060744	0.001265	584	25	557	18	630	45	88	564	33.45	1.04	0.31	38	46	0.818
oc26a71	0.674801	0.050771	0.088672	0.003076	0.230495	0.057346	0.001021	524	31	548	18	505	39	108	543	34.04	0.58	0.45	41	65	0.626
oc26a72	0.733719	0.051124	0.089279	0.003468	0.278763	0.062670	0.001391	559	30	551	21	697	47	79	553	37.84	0.06	0.81	30	44	0.691
oc26a73	0.628764	0.060593	0.090248	0.004225	0.242877	0.055096	0.001374	495	38	557	25	416	56	134	540	45.43	2.47	0.12	17	28	0.597
oc26a78	0.715515	0.039154	0.088667	0.002555	0.263286	0.059024	0.001038	548	23	548	15	568	38	96	548	28.06	0.00	0.99	42	57	0.737
oc26a79	0.719780	0.038476	0.089343	0.002809	0.294131	0.059194	0.000974	551	23	552	17	574	36	96	551	30.23	0.00	0.96	48	68	0.701
oc26a80	0.703541	0.039155	0.092311	0.002649	0.257796	0.058389	0.001055	541	23	569	16	544	39	105	562	28.63	1.35	0.25	40	58	0.696
oc26a81	0.657010	0.041842	0.089977	0.002625	0.229079	0.055127	0.001069	513	26	555	16	417	43	133	546	28.79	2.60	0.11	35	54	0.643
oc26a82	0.767298	0.037891	0.088937	0.002621	0.298440	0.062013	0.001109	578	22	549	16	675	38	81	557	28.61	1.61	0.20	28	42	0.651
oc26a83	0.675687	0.055658	0.092485	0.003183	0.208934	0.056645	0.001368	524	34	570	19	478	53	119	561	35.19	1.78	0.18	27	38	0.718

mafic schists in Coachman's Harbour (Fig. 4A). The strain is heterogeneous and low-strain pods locally preserve primary igneous subophitic textures that are pseudomorphed by greenschist to albite – amphibolite facies mineral assemblages (Fig. 5B). Two samples of metagabbro were collected in Coachman's Harbour (Fig. 2). They comprise a relatively weakly strained, coarse-grained leucogabbro pod described in detail in Hibbard (1983, p. 49) (SNB-06-017; Fig. 5) and the enveloping schistose metagabbro (DC 09/08-30; Fig. 6). The low-strain leucogabbro (sample SNB-06-017, z9251) yielded abundant high quality zircon grains (100 to 200 μm) including delicate elongate crystals, prismatic grains, and flat, tabular fragments. Six single-grain and multigrain fractions were analyzed using U–Pb ID–TIMS. All six analyses overlap on concordia and each other (Table 1; Figure 4A) and yield a weighted average $^{206}Pb/^{238}U$ age of 558.0 ± 0.5 Ma (mean square weighted deviation (MSWD) = 0.73; probability of fit = 0.60). A concordia age, with decay-constant errors included, is calculated to be 558.3 ± 0.7 Ma (MSWD of concordance and equivalence = 1.5, probability = 0.14, n = 6). The age of 558.3 ± 0.7 Ma (Fig. 5A) is interpreted to be the crystallization age of the Birchy Complex leucogabbro.

The schistose metagabbro (DC 09/08-30) yielded a homogenous population of short prismatic zircons up to 100 μm. Cathodoluminescence imaging revealed homogenous grain interiors or oscillatory idiomorphic growth zoning (e.g. Fig. 6A) and common very thin (< 10 μm) low U rims. LA–ICPMS analysis of the cores of fourteen zircon grains yielded a concordia age of 563.9 ± 7.5 Ma (MSWD = 0.89; Fig. 6D), interpreted to represent the crystallization age of the metagabbro. This age is within analytical uncertainty of the ID–TIMS U–Pb zircon age.

Tuffaceous Schist

The Birchy Complex mafic to intermediate schist was sampled along the coast ca. 1 km south of Coachman's Harbour. The sampled locality is characterized by a thin, brown-weathering, tuffaceous schist of mafic to interme-

diate composition (DC09/08-41) cut by gabbroic sheets (Fig. 4E). The zircon population comprises small (between 75–150 μm in diameter), stubby prismatic zircons, with aspect ratios between 1.5 and 3.0. The grains typically exhibited only minor rounding, but were commonly fractured. Cathodoluminescence imaging revealed predominantly homogenous grain interiors (Fig. 6B) displaying local oscillatory idiomorphic growth zoning (e.g. Fig. 6C). LA–ICPMS analysis of 51 spots on separate grains yielded a concordia age of 556.3 ± 3.6 Ma and a weighted mean $^{206}Pb/^{238}U$ age of 556.4 ± 3.5 Ma (MSWD = 0.61; Fig. 6E, F). This is within analytical uncertainty of the ID–TIMS and LA–ICPMS U–Pb zircon ages of the intrusive metagabbros, suggesting that all mafic to intermediate schists of the Birchy Complex are consanguineous and have a Late Ediacaran age of ca. 558 Ma.

Flat Point Formation Psammite

The Flat Point Formation was formerly included with the Rattling Brook Group, but following Kennedy (1971) is interpreted as a stratigraphic cover to the Birchy Complex. A psammite of the Flat Point Formation (DC 09/08-34) was sampled for U–Pb detrital zircon analysis. In general, most of the detrital zircons analyzed (Fig. 6G) yield Mesoproterozoic ages (1.0 – 1.5 Ga), and display a prominent Grenvillian peak typical of the Laurentian basement widely exposed in the Grenville province of southern Labrador and unconformably underlying parts of the Humber margin in western Newfoundland (Heaman et al. 2002; Gower et al. 2008). Smaller Paleoproterozoic (1.8 – 2.0 Ga) and Neoarchean (2.4 – 3.0 Ga) peaks are also consistent with a proximal Laurentian provenance. The youngest detrital zircon yielded a U–Pb concordia age of 990 ± 52 Ma.

Metamorphosed correlatives of the Fleur de Lys rocks in west-central Newfoundland (Hibbard 1988) yield a very similar Precambrian age distribution that corresponds closely to those measured by Cawood and Nemchin (2001).

GEOCHEMISTRY OF THE BIRCHY SCHIST

Analytical Methods

Mafic and ultramafic rocks prefaced by DC were analyzed for major oxides and trace elements by X-ray fluorescence (XRF) spectroscopy using a Phillips PW 1400 at the Centre d'Analyses Minérale, University of Lausanne, Switzerland (Table 3). Samples were fused with lithium borate and analysed for their major, trace element and rare-earth element concentrations by inductively coupled plasma optical emission spectrometry (ICPOES) and ICPMS (Thermo X-Series) at OMAC Laboratories, County Galway, Ireland. Where there are both ICP and XRF data for the same element, the ICP data are generally preferred, particularly for elements with low abundances such as U, Pb, Th, Ba, and the rare-earth elements (REEs) (Table 3). Samples prefaced by SNB were fused with lithium borate and analysed for their major, trace element and rare-earth element concentrations by ICPOES and ICPMS at Activation Laboratories in Ancaster, Ontario (Table 4).

A subset of samples was selected for Nd isotopic analysis utilizing a Thermo – Finnigan Triton T1 thermal ionization mass spectrometer at Carleton University, Ottawa, Ontario (Table 5). REE fractions were dissolved in 0.26N HCl and loaded onto Eichrom Ln Resin chromatographic columns containing Teflon powder coated with HDEHP (di(2-ethylhexyl) orthophosphoric acid; Richard et al. 1976). Nd was eluted using 0.26N HCl, followed by Sm in 0.5N HCl. Total procedural blanks for Nd are < 50 picograms, and < 6 picograms for Sm. Samples were spiked with a mixed ^{148}Nd–^{149}Sm spike prior to dissolution. Concentrations are precise to +/- 1%, while $^{147}Sm/^{144}Nd$ ratios are reproducible to 0.5%. Samples were loaded with H_3PO_4 on one side of a Re double filament, and run at temperatures of 1700–1800° C. Isotope ratios are normalized to $^{146}Nd/^{144}Nd$ = 0.72190. Analyses of the USGS standard BCR-1 yield Nd = 29.02 ppm, Sm = 6.68 ppm, and $^{143}Nd/^{144}Nd$ = 0.512668 +/- 20 (n=4). The international La Jolla standard yielded $^{143}Nd/^{144}Nd$ = 0.511847 +/- 7, n = 26 (February 2005 – June 2007). Internal lab Nd standard yielded 0.511819 +/- 10 n = 94 (February 2005 – August 2009) and 0.511823 +/- 12 n = 65 (October 2010 – July 2012).

Birchy Complex Mafic Rocks

Hibbard (1983) determined that mafic rocks of the Birchy Complex are tholeiitic (Fig. 7A) and have a strong affinity with MORB. Although there is an apparent overlap with mafic rocks in the structurally overlying Baie Verte oceanic tract (BVOT), Hibbard (1983) observed that the Birchy Complex greenschists are commonly slightly enriched in TiO_2 compared to the adjacent BVOT rocks of the Advocate Complex. Overall, analysis of the Birchy Complex mafic rocks confirms the observations of Hibbard (1983). Two geochemical suites of mafic rocks can be readily identified on the basis of major and trace element data. All mafic rocks have relatively flat rare-earth element patterns on a MORB-normalised diagram, but the first suite (metagabbro) is characterized by lower TiO_2, Zr depletion and Eu enrichment on a MORB-normalized profile (Fig. 7B). The second suite, consisting of typically fine-grained mafic rocks interpreted as metabasalt, is characterized by higher TiO_2, small to negligible Nb and La anomalies, and enrichment of Th relative to Nb (Fig. 7B). Both suites plot in the MORB field adjacent to the field of backarc basin basalt on a La–Y–Nb tectonic discrimination diagram (Fig. 7C). Sm–Nd isotopic analyses yielded εNd values of +7.4 and +7.2 respectively (Fig. 8).

Birchy Complex Intermediate Tuff

A sample of intermediate tuffaceous schist plots in the dacite – rhyolite field on a Zr/Ti vs. Nb/Y diagram (Fig. 7A). The sample is characterized by slight light REE enrichment, positive Zr and Hf anomalies, and negative Eu and Ti anomalies (Fig. 7B). Similar to the mafic rocks, the intermediate tuff lacks prominent La and Nb anomalies but has a strong Th enrichment. It plots in the ocean ridge granite field on granitoid tectonic discrimination plots of Pearce et al. (1984; not shown). Sm–Nd isotopic analysis of the tuff yielded εNd value of +7.5 (Fig. 8).

Table 3. Whole rock geochemical data (major, trace and rare earth elements) for the Birchy Complex (samples prefaced by DC). ICP and XRF data are provided for the each sample. See text for methods used.

Sample	DC 09/08/21	DC 09/08/22	DC 09/08/23	DC 09/08/24	DC 09/08/25	DC 09/08/26	DC 09/08/27	DC 09/08/29	DC 09/08/30	CD 09/08/31
Description	metabasalt	metabasalt	coticule	serpentinite	serpentinite	metabasalt	metabasalt	metabasalt	metabasalt	metabasalt
Symbol[1]	1	1	NP	3	3	2	2	2	2	1
Latitude	50.05297	50.05067	50.05002	50.04832	50.04852	50.05017	50.05018	50.05001	50.04999	50.05061
Longitude	-56.09827	-56.10709	-56.10681	-56.10826	-56.10816	-56.11256	-56.11231	-56.11176	-56.11186	-56.11373
ICP-OES, ICP-MS										
SiO_2 (wt%)	48.18	43.76	43.66	55.76	36.87	48.47	49.97	48.51	49.51	47.33
Al_2O_3	13.08	13.88	8.92	1.64	1.21	12.75	14.88	16.15	16.80	13.26
CaO	10.57	8.08	2.75	12.52	1.20	11.84	11.85	10.83	11.48	8.85
Cr_2O_3	0.01	0.03	0.00	0.24	0.34	0.03	0.05	0.03	0.04	0.01
Fe_2O_3	15.26	15.59	27.96	5.18	7.50	10.87	9.52	9.59	7.82	16.41
K_2O	0.01	0.58	1.77	0.38	0.05	0.07	0.09	0.07	0.07	0.14
MgO	7.08	7.57	2.74	21.49	38.16	9.47	8.17	6.97	6.67	6.43
MnO	0.24	0.21	5.21	0.16	0.08	0.18	0.18	0.15	0.14	0.22
Na_2O	1.17	2.94	0.60	0.85	1.09	3.55	4.59	4.82	4.91	4.00
P_2O_5	0.20	0.17	0.17	<0.01	0.03	0.03	0.05	0.08	0.08	0.30
TiO_2	1.88	1.96	0.54	0.01	<0.01	0.71	0.75	0.98	0.64	2.52
LOI (1000ºC)	2.91	3.16	4.74	2.21	12.82	2.33	2.46	2.23	1.95	2.80
Ba (ppm)	4.92	26.40	238.54	50.60	0.92	4.45	6.58	4.29	5.30	8.31
Ce	13.62	14.63	453.70	0.66	<0.5	4.00	4.26	6.01	4.80	22.52
Dy	6.33	6.76	13.05	<0.1	<0.1	2.82	2.81	3.75	2.66	9.35
Er	4.34	4.45	6.58	<0.1	<0.1	1.94	1.87	2.55	1.76	6.26
Eu	1.41	1.54	3.19	<0.1	<0.1	0.70	0.70	0.92	0.69	2.06
Ga	18.90	18.95	12.88	3.40	2.08	14.70	14.44	14.83	14.44	19.77
Gd	5.05	5.60	18.88	<0.1	<0.1	2.12	2.11	2.92	2.05	7.99
Hf	2.33	2.84	2.66	<1	<1	<1	<1	1.11	<1	4.46
Ho	1.46	1.51	2.46	<0.1	<0.1	0.65	0.63	0.87	0.59	2.12
La	5.02	5.15	105.19	<0.5	<0.5	1.30	1.47	2.10	1.66	7.81
Lu	0.68	0.64	0.79	<0.1	<0.1	0.30	0.28	0.36	0.27	0.97
Nb	3.98	4.04	7.88	<0.5	<0.5	1.13	1.22	1.75	1.25	6.38
Nd	11.40	12.46	98.68	<0.5	<0.5	3.88	4.10	5.51	4.28	18.88
Pr	2.19	2.39	25.98	<0.1	<0.1	0.69	0.73	1.01	0.80	3.72
Rb	<0.5	14.39	119.61	7.05	<0.5	<0.5	<0.5	<0.5	<0.5	0.65
Sc	51.94	51.42	24.74	4.13	9.38	53.09	51.34	49.60	40.71	51.21
Sm	3.83	4.39	20.28	<0.1	<0.1	1.60	1.54	2.06	1.57	6.29
Sn	<1	1.36	1.61	<1	<1	<1	<1	<1	<1	<1
Sr	145.85	118.34	200.81	6.90	13.29	94.22	100.44	108.54	123.54	96.59
Ta	0.22	0.24	0.55	0.12	<0.1	0.13	0.12	0.24	0.13	0.42
Tb	1.00	1.07	2.69	<0.1	<0.1	0.43	0.42	0.57	0.41	1.48
Th	0.47	0.34	18.95	<0.1	<0.1	<0.1	<0.1	<0.1	<0.1	0.52
Tm	0.66	0.67	0.88	<0.1	<0.1	0.28	0.28	0.39	0.26	1.00
U	0.20	0.17	1.08	<0.1	<0.1	<0.1	<0.1	<0.1	<0.1	0.20
V	434.67	409.89	360.84	30.78	33.60	265.20	257.02	265.32	193.38	499.80
W	5.10	3.63	1.65	<0.5	11.30	8.57	4.85	5.14	19.22	1.33
Y	42.08	42.83	59.60	0.62	<0.5	17.81	17.45	23.99	17.31	63.14
Yb	4.23	4.40	5.35	<0.1	<0.1	1.91	1.79	2.45	1.78	6.26
Zr	83.08	100.28	121.37	5.71	2.54	25.45	33.17	39.87	31.52	172.68
XRF										
SiO_2 (wt%)	48.81	45.70	45.33	57.17	39.33	50.01	50.46	50.01	51.50	47.67
TiO_2	1.90	2.07	0.59	0.01	0.02	0.74	0.76	0.99	0.66	2.49
Al_2O_3	13.05	14.33	9.33	1.84	1.44	12.91	14.79	16.29	16.88	13.03
Fe_2O_3	14.50	15.52	27.26	4.86	7.38	10.67	8.94	9.30	7.81	16.00
MnO	0.24	0.22	5.54	0.17	0.09	0.20	0.19	0.17	0.16	0.24
MgO	7.01	7.58	2.67	21.13	37.64	9.60	8.15	7.25	6.64	6.31
CaO	10.24	8.20	2.83	12.60	1.21	11.78	11.70	11.04	11.48	8.66
Na_2O	1.13	2.73	0.15	0.00	0.00	2.00	2.75	2.98	3.27	2.38
K_2O	0.03	0.60	1.79	0.34	0.00	0.04	0.05	0.04	0.04	0.09
P_2O_5	0.18	0.18	0.18	0.01	0.01	0.05	0.06	0.09	0.06	0.29
LOI	2.66	2.80	3.43	2.00	12.42	2.04	2.09	1.98	1.77	2.54
Cr_2O_3	0.02	0.04	0.01	0.23	0.34	0.04	0.05	0.04	0.04	0.02
NiO	0.01	0.02	0.03	0.14	0.25	0.01	0.01	0.01	0.01	0.01
Sum	99.78	100.01	99.14	100.50	100.13	100.09	100.00	100.19	100.32	99.73
Nb (ppm)	10	10	17	7	9	6	5	5	5	13
Zr	97	110	100	14	22	34	36	51	43	177
Y	34	34	32	6	5	19	20	24	21	48
Sr	134	113	212	7	11	88	93	106	116	93
U	<2<	<2<	2	2	<2<	<2<	<2<	<2<	<2<	4
Rb	4	17	82	11	4	4	4	4	4	6
Th	<2<	3	26	3	<2<	<2<	<2<	<2<	<2<	5
Pb	<2<	<2<	47	8	10	<2<	<2<	<2<	<2<	2
Ga	20	20	16	6	5	17	16	18	16	23
Zn	130	133	138	44	36	84	81	61	66	127
Cu	70	33	143	14	<2<	8	6	50	4	54
Ni	50	145	335	649	911	79	81	71	64	50
Co	52	56	95	33	95	44	41	35	34	46
Cr	95	328	23	1512	2412	275	407	301	305	103
V	441	475	450	25	55	278	247	233	193	547
Ce	7	10	<3<	<3<	<3<	<3<	3	9	8	19
Nd	5	8	<4<	6	5	<4<	<4<	7	7	7
Ba	<9<	23	173	59	11	<9<	<9<	<9<	12	<9<
La	5	10	60	<4<	<4<	<4<	<4<	9	<4<	6
S	1124	197	38044	169	5635	140	129	181	120	4525
Hf	6	1	<1<	<1<	<1<	<1<	<1<	3	<1<	3
Sc	53	78	53	16	41	51	42	35	33	75
As	<3<	4	6	15	17	<3<	<3<	4	<3<	<3<

Note: [1] Symbols in figures 6 and 7 are 1 - filled triangle, 2 - open triangle, 3 - filled square, 4 - filled diamond, NP - not plotted.

(continued)

Table 3. (*Concluded*) Whole rock geochemical data (major, trace and rare earth elements) for the Birchy Complex (samples prefaced by DC). ICP and XRF data are provided for the each sample. See text for methods used.

Sample	DC 09/08/32	DC 09/08/33	DC 09/08/35	DC 09/08/36	DC 09/08/37	DC 09/08/38	DC 09/08/39	DC 09/08/40	CD 09/08/41	CD 09/08/42
Description	serpentinite	metabasalt	serpentinite	serpentinite	metabasalt	metabasalt	metabasalt	metabasalt	inter. tuff	metabasalt
Symbol[1]	3	1	3	3	1	2	1	1	4	2
Latitude	50.05495	50.05495	50.0606	50.06022	50.06124	50.04611	50.04485	50.04035	50.04035	50.03504
Longitude	-56.11515	-56.11515	-56.11192	-56.11713	-56.1155	-56.11238	-56.11123	-56.11406	-56.11406	-56.11978
ICP-OES, ICP-MS										
SiO_2 (wt%)	54.15	46.24	52.25	53.20	45.21	50.02	47.88	47.63	59.86	49.80
Al_2O_3	0.93	12.63	2.00	6.09	14.58	16.90	13.63	12.99	11.05	17.38
CaO	13.19	8.32	12.21	10.38	10.04	11.49	10.73	9.01	5.18	14.14
Cr_2O_3	0.07	0.02	0.32	0.40	0.03	0.04	0.03	0.02	<0.001	0.07
Fe_2O_3	5.52	14.13	6.58	8.19	12.18	7.85	14.80	15.22	12.80	6.06
K_2O	0.08	0.15	0.20	2.00	0.38	0.07	0.07	0.08	0.61	0.06
MgO	21.01	7.22	19.37	16.73	6.93	6.86	7.12	7.11	1.21	8.20
MnO	0.23	0.23	0.17	0.19	0.18	0.14	0.22	0.25	0.11	0.12
Na_2O	1.65	4.70	1.89	1.38	4.35	4.49	3.90	3.55	3.99	3.00
P_2O_5	0.02	0.21	0.02	<0.01	0.17	0.06	0.17	0.19	0.18	0.02
TiO_2	0.04	1.58	0.03	0.04	1.72	0.64	1.86	2.12	0.75	0.33
LOI (1000ºC)	3.15	3.18	2.63	2.28	5.00	2.10	1.94	2.36	2.68	1.67
Ba (ppm)	0.57	8.55	12.82	270.44	28.15	31.23	8.61	9.36	449.66	6.45
Ce	2.25	12.18	4.02	<0.5	13.17	3.11	13.30	15.58	112.33	1.03
Dy	0.26	5.51	0.11	<0.1	5.87	2.39	6.28	7.41	39.18	1.25
Er	0.18	3.72	<0.1	<0.1	3.72	1.51	4.18	5.02	27.66	0.87
Eu	<0.1	1.22	<0.1	<0.1	1.49	0.59	1.48	1.69	4.99	0.40
Ga	2.29	15.18	3.98	8.32	15.12	14.85	18.98	18.07	23.61	14.23
Gd	0.24	4.35	0.21	<0.1	4.89	1.76	5.16	6.09	31.93	0.94
Hf	<1	2.19	<1	<1	2.70	<1	2.72	3.35	31.86	<1
Ho	<0.1	1.25	<0.1	<0.1	1.29	0.55	1.45	1.70	9.03	0.31
La	0.99	4.12	2.38	<0.5	4.35	1.00	4.68	5.32	37.21	<0.5
Lu	<0.1	0.58	<0.1	<0.1	0.56	0.24	0.63	0.78	4.49	0.14
Nb	<0.5	2.87	<0.5	<0.5	2.33	0.80	3.95	4.36	30.88	0.52
Nd	1.00	9.65	1.89	<0.5	11.69	3.11	11.85	13.98	90.40	1.28
Pr	0.27	1.85	0.48	<0.1	2.30	0.56	2.25	2.66	18.24	0.20
Rb	<0.5	1.78	2.77	43.35	5.57	3.84	<0.5	<0.5	23.51	<0.5
Sc	5.82	45.98	1.30	8.23	41.58	47.73	50.36	50.26	18.10	48.36
Sm	0.22	3.34	0.24	<0.1	3.92	1.27	4.06	4.69	26.79	0.61
Sn	<1	<1	1.10	<1	1.20	<1	<1	<1	1.07	<1
Sr	53.00	104.22	43.60	13.50	181.42	146.08	107.18	78.29	246.87	109.92
Ta	<0.1	0.24	<0.1	<0.1	0.18	<0.1	0.29	0.32	2.34	<0.1
Tb	<0.1	0.86	<0.1	<0.1	0.93	0.36	1.00	1.14	6.17	0.20
Th	<0.1	0.23	<0.1	<0.1	0.14	<0.1	0.26	0.27	6.03	<0.1
Tm	<0.1	0.57	<0.1	<0.1	0.57	0.23	0.62	0.76	4.47	0.13
U	0.14	0.12	<0.1	<0.1	0.13	<0.1	0.12	0.13	1.57	<0.1
V	43.05	383.57	28.64	100.39	301.36	232.80	397.88	463.30	6.93	187.55
W	<0.5	5.42	<0.5	1.13	2.30	6.35	3.73	5.66	7.66	9.68
Y	2.02	34.27	1.14	0.66	36.17	14.94	41.27	48.65	270.00	8.67
Yb	0.23	3.69	0.13	0.10	3.68	1.55	4.17	4.96	29.10	0.88
Zr	7.80	74.27	4.66	2.73	99.33	22.43	97.00	120.65	1179.88	17.83
XRF										
SiO_2 (wt%)	56.48	47.87	54.93	53.99	46.51	49.13	47.79	48.38	62.75	50.61
TiO_2	0.02	1.63	0.02	0.05	1.74	0.64	1.87	2.15	0.74	0.33
Al_2O_3	1.07	12.91	2.17	6.25	14.81	16.13	13.27	12.87	11.13	17.30
Fe_2O_3	5.34	13.96	6.32	7.78	11.79	6.84	13.97	14.58	12.39	5.84
MnO	0.25	0.24	0.19	0.20	0.19	0.13	0.23	0.26	0.12	0.13
MgO	21.01	7.37	19.45	16.10	6.94	7.98	6.94	7.09	1.10	8.12
CaO	13.45	8.50	12.73	10.26	10.01	14.35	10.45	9.02	5.10	14.23
Na_2O	0.00	3.45	0.32	0.00	3.21	1.79	2.60	2.30	2.83	2.02
K_2O	0.01	0.11	0.16	1.95	0.34	0.20	0.08	0.06	0.58	0.04
P_2O_5	0.01	0.16	0.01	0.01	0.16	0.04	0.18	0.22	0.19	0.01
LOI	2.85	2.93	2.39	2.09	4.56	1.83	1.74	2.23	2.32	1.49
Cr_2O_3	0.08	0.02	0.30	0.39	0.03	0.12	0.03	0.02	0.00	0.07
NiO	0.06	0.01	0.14	0.11	0.01	0.02	0.01	0.01	0.00	0.01
Sum	100.63	99.15	99.12	99.17	100.31	99.18	99.15	99.20	99.25	100.18
Nb (ppm)	7	9	7	6	7	3	9	10	36	2
Zr	12	84	12	12	121	32	105	116	850	14
Y	8	30	6	7	33	18	34	38	191	13
Sr	49	101	40	13	175	137	102	72	231	98
U	<2<	2	<2<	<2<	<2<	<2<	<2<	<2<	<2<	2
Rb	4	5	7	47	10	9	4	5	22	5
Th	6	2	4	2	3	2	3	2	8	<2<
Pb	339	<2<	53	3	<2<	<2<	<2<	2	6	<2<
Ga	6	18	8	11	18	16	21	21	23	16
Zn	59	123	92	98	89	49	96	125	37	37
Cu	<2<	98	<2<	<2<	69	107	3	35	153	16
Ni	291	60	761	647	78	112	67	66	8	91
Co	32	56	38	59	46	31	51	47	22	30
Cr	501	138	2294	2799	241	841	220	177	<2<	592
V	46	451	24	113	349	230	440	500	<2<	191
Ce	7	14	4	<3<	16	4	6	6	23	4
Nd	7	8	4	<4<	12	5	4	<4<	<4<	5
Ba	<9<	<9<	17	299	16	28	<9<	<9<	481	<9<
La	<4<	5	16	<4<	7	4	<4<	6	17	<4<
S	398	441	152	355	260	259	120	305	7429	143
Hf	<1<	<1<	<1<	<1<	2	<1<	<1<	<1<	22	<1<
Sc	18	70	15	15	46	25	62	67	21	26
As	10	<3<	6	215	6	7	3	5	8	<3<

Note: [1] Symbols in figures 6 and 7 are 1 - filled triangle, 2 - open triangle, 3 - filled square, 4 - filled diamond, NP - not plotted.

Table 4. Whole rock geochemical data for the Birchy Complex (samples prefaced by SNB). See text for methods used.

Sample	SNB 08 E 005 A1	SNB 08 E 006 A2	SNB 08 E 006 A3	SNB 08 E 004 A1	SNB 08 E 006 A1
Description	serpentinite	serpentinite	serpentinite	serpentinite	serpentinite
Symbol[1]	3	3	3	3	3
Latitude	50.051	50.118	50.118	50.051	50.118
Longitude	-56.105	-56.125	-56.125	-56.105	-56.125
ICP-OES, ICP-MS					
SiO_2 (wt%)	40.08	40.32	39.32	41.88	40.49
Al_2O_3	1.71	0.52	0.62	0.94	0.49
Cr_2O_3	0.31	0.4	0.28	0.29	0.29
Fe_2O_3	7.92	7.22	6.1	6.99	5.31
MnO	0.065	0.065	0.073	0.077	0.058
MgO	37.16	39.54	39.25	36.53	38.95
CaO	1.16	0.57	0.13	0.62	0.43
Na_2O	0.14	0.04	< 0.01	0.04	0.05
K_2O	0.03	0.03	0.06	0.11	0.03
TiO_2	0.037	0.003	0.011	0.021	0.009
P_2O_5	< 0.01	< 0.01	< 0.01	< 0.01	< 0.01
LOI (1000°C)	12.66	12.33	13.08	11.89	14.63
Sum	101	100.6	98.65	99.1	100.5
Ba (ppm)	4	< 3	< 3	290	106
Ce	0.62	< 0.05	0.06	4.16	1.34
Co	90	90	92	107	87
Cs	< 0.1	< 0.1	< 0.1	< 0.1	0.5
Cu	10	40	< 10	< 10	< 10
Dy	0.18	0.02	< 0.01	0.16	0.06
Er	0.13	0.01	0.01	0.1	0.04
Eu	0.024	< 0.005	< 0.005	0.021	0.011
Gd	0.13	0.02	< 0.01	0.21	0.08
Hf	< 0.1	< 0.1	0.1	0.2	< 0.1
Ho	0.04	< 0.01	< 0.01	0.03	0.01
La	0.79	0.3	0.61	2.43	1.01
Lu	0.023	0.004	0.003	0.012	0.008
Nb	0.5	0.3	< 0.2	< 0.2	0.5
Nd	0.35	0.07	< 0.05	1.53	0.62
Ni	1720	1770	2230	2210	2100
Pb	6	< 5	< 5	15	< 5
Pr	0.08	0.02	< 0.01	0.47	0.17
Rb	1	< 1	< 1	< 1	3
Sc	10	8	8	8	6
Sm	0.09	0.02	< 0.01	0.29	0.13
Sr	15	17	6	23	33
Ta	< 0.01	< 0.01	< 0.01	0.03	< 0.01
Tb	0.03	< 0.01	< 0.01	0.03	0.01
Th	0.13	< 0.05	< 0.05	1.33	0.65
Tm	0.02	< 0.005	< 0.005	0.015	0.008
U	3.64	0.35	0.02	5	2.14
V	38	14	18	22	12
Y	1.2	< 0.5	< 0.5	0.9	< 0.5
Yb	0.14	0.03	0.02	0.08	0.05
Zr	8	< 1	7	9	4

Note: [1] Symbols in Figure 6 are filled squares

Ultramafic Rocks

The ultramafic rocks in the Birchy Complex and Rattling Brook Group are generally highly metamorphosed and strongly metasomatised to serpentinite, listwanite, soapstone and actinolite – fuchsite schist. The sampled serpentinites and actinolite – fuchsite schist locally preserve relict igneous minerals; soapstone, listwanite and carbonate – tremolite bearing ultramafic schists were not sampled due to extensive metasomatism. The pervasive degree of alteration of the ultramafic samples complicates interpretation of primary lithologies; however, Niu (2004) demonstrated that the bulk compositions of pervasively hydrated peridotites can preserve primary magmatic signatures. Normative calculations (not shown) suggest that the protoliths to the serpentinites were harzburgite and dunite, consistent with presence of relict orthopyroxene in some samples. Presence of minor normative clinopyroxene may suggest that some of the samples may be lherzolitic; however, this can also be attributed to introduction of silica and minor hydrothermal calcium during serpentinization. The actinolite – fuchsite schists are petrographically distinct from serpentinites and most likely represent hydrated websterite and/or pyroxenite.

Trace element abundances in harzburgites and websterites are very low and commonly near or below the detection limit for the analytical techniques used in this study, resulting in missing elements (below detection limit) or jagged patterns (near detection limit; Fig. 7D). All ultramafic rocks are characterized by depleted heavy REE relative to primitive mantle (Fig. 7D). All samples display strong light REE enrichment, similar to metasomatized mantle of the BVOT, but distinct from abyssal and forearc peridotites (Fig. 7D). Most analysed serpentinites probably represent altered metasomatised mantle. However, negative Eu and Ti anomalies for some samples (SNB 08 004A1 and 006A1) indicate that these may represent lower crustal cumulate.

IMPLICATIONS OF THE U–PB ZIRCON DATA AND GEOCHEMISTRY FOR THE TECTONIC SETTING OF THE BIRCHY COMPLEX AND ASSOCIATED ROCKS

The Birchy Complex, correlatives in the Mings Bight Group (Fig. 1) and mafic – ultramafic rocks in the Rattling Brook Group were previously interpreted as dismembered slices of relatively old Iapetan oceanic lithosphere (Fig. 3; Hibbard 1988). However, no evidence for formation by magmatically active seafloor spreading, such as abundant pillow lavas, sheeted dikes and mafic – ultramafic cumulates typically found at the base of true oceanic crust, has been preserved. The subsequent strong Taconic and Salinic tectonic overprints (van Staal et al. 2009 a, b; Castonguay et al. 2010) could have destroyed all such primary features, although this would be surprising considering the heterogeneous nature of the deformation (see above). More significantly, the age data presented herein are inconsistent with

Table 5. Sm–Nd isotopic characteristics of the Birchy Complex

Sample	Description	Age (Ma)	Nd (ppm)[1]	Sm (ppm)[1]	$^{143}Nd/^{144}Nd$[1]	$^{147}Sm/^{144}Nd$[1]	$^{143}Nd/^{144}Nd$[2]	εNd[2]
06-SNB-017	metagabbro	560	6.06	2.30	0.513124	0.2294	0.512282	7.2
07-SNB-S170A-01	psammite	560	59.4	11.2	0.511943	0.1144	0.511523	-7.7
DC-09-08-31	metabasalt	560	20.1	6.68	0.513034	0.2012	0.512296	7.4
DC-09-08-41	intermediate tuff	560	94.2	28.6	0.512975	0.1832	0.512303	7.5

Notes: [1] – measured; [2] – calculated following DePaolo (1981)

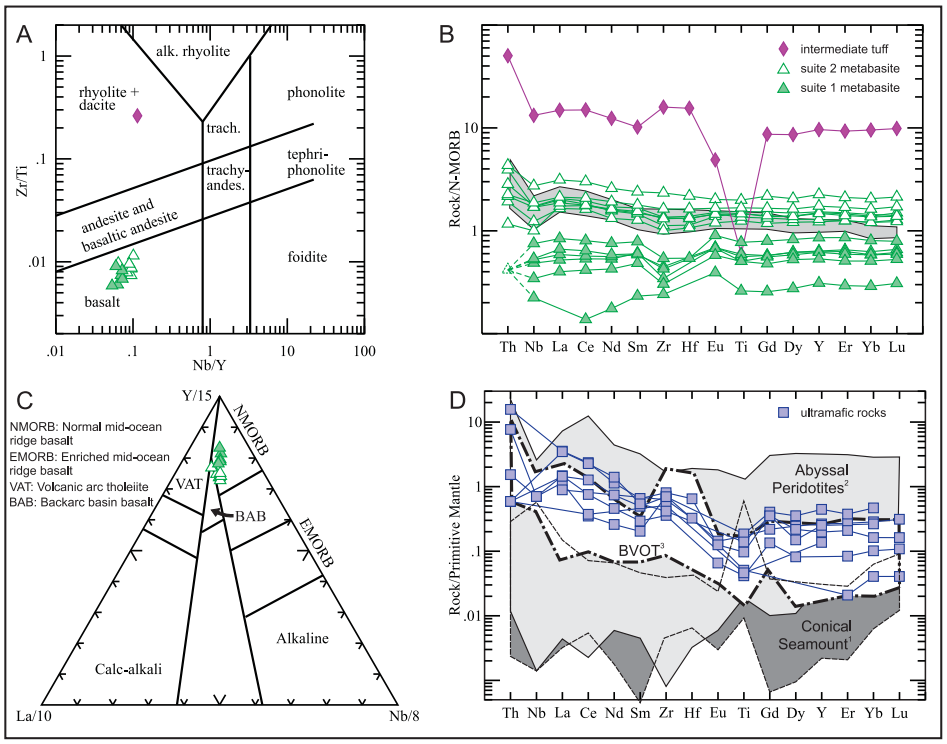

Figure 7. Geochemical characteristics of the Birchy Complex. A. Zr/Ti vs. Nb/Y rock type discrimination plot (Pearce 1996). Mafic rocks are tholeiitic basalts. B. NMORB-normalized (Sun and McDonough 1989) multi-element diagram for mafic and intermediate rocks. Dashed lines indicate samples where Th is plotted at half the detection limit. For reference, the composition of Cretaceous basalts (mainly sheet flows) erupted along the distal part of the Newfoundland rifted margin (ocean – continent transition) are plotted in the grey band (Robertson 2007). C. La–Y–Nb tectonic setting discrimination plot (Cabanis and Lecolle 1989) for mafic rocks of the Birchy Complex. D. Primitive mantle-normalized (Sun and McDonough 1989) multi-element diagram for ultramafic rocks (1 – Savov et al. 2005; 2– Niu 2004; 3 – Baie Verte oceanic tract (BVOT) – Bédard and Escayola 2010).

such an interpretation, because they show that the bulk of the Birchy Complex is Late Ediacaran. The Birchy Complex thus overlaps temporally with the last phase of rift-related magmatism in this sector of the Laurentian margin and significantly predates (30–40 my) the late Early Cambrian thermal subsidence-related transgression, commonly used as a proxy for the final rift-drift event along the Humber margin (Cawood et al. 2001; Waldron and van Staal 2001). The age of the ultramafic rocks in both the Rattling Brook Group and Birchy Complex is unknown, but the presence of ultramafic-derived chromite in the enclosed sedimentary rocks and their close spatial association with the mafic rocks (Fig. 4A) indicates that they are pre-Late Ediacaran.

The Precambrian age distribution of the detrital zircons of the Flat Point Formation corresponds closely to correlatives of the Fleur de Lys rocks in west-central Newfoundland (Hibbard 1988; Cawood and Nemchin 2001). The continental isotopic signature of the sediments intercalated with the Birchy Complex (εNd = -7.7; Table 5) and the typical Laurentian zircon provenance of the Flat Point formation (Fig. 6G) support the proximity of the Birchy Complex to the Humber margin, as suggested by Hibbard (1983). The age, provenance and isotopic characteristics presented herein support formation of the Birchy Complex during the extension and final rifting event along the Humber margin, shortly before the onset of oceanic spreading further outboard. The age of the Flat Point Formation and the age of the Rattling Brook Group in general, are poorly constrained at present. The youngest detrital zircon in the Flat Point Formation yielded a U–Pb concordia age of 990 ± 52 Ma. The presence of mafic intrusive and extrusive rocks with compositions similar to those found in the rift sequence of the Labrador Group (de Wit and Strong 1975; Hibbard 1983) suggests that the associated sedimentary rocks of the Rattling Brook Group and other correlative units of the Fleur de Lys Supergroup are probably also Ediacaran and therefore form part of the rift sequence.

The presence of marble and calcareous rocks in other parts of the Rattling Brook Group and also in the Flat Point Formation, suggests that these units were probably mainly deposited during the drift stage. The drift stage is constrained to be Early Cambrian to Early Ordovician (Cawood et al. 2001); hence, this part of the Rattling Brook Group is younger than the Birchy Complex. Based on the apparent stratigraphic contacts between the Birchy Complex and overlying Flat Point Formation, we interpret the latter to have been deposited above the Birchy Complex during the Early Cambrian, following

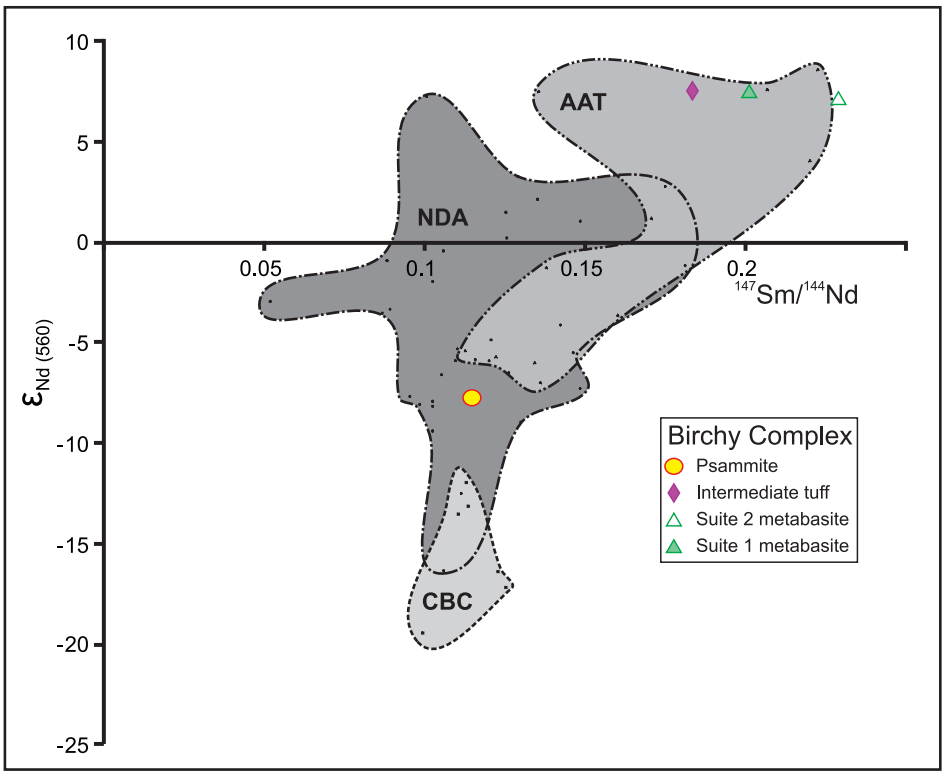

Figure 8. Sm–Nd isotopic characteristics of the Birchy Complex (sample key is same as in Fig. 7) and comparison to the Achill Beg Formation, Clew Bay Complex (CBC), Ireland (Chew 2003), Notre Dame Arc (NDA), Newfoundland (Whalen et al. 1997); and Annieopsquotch Accretionary Tract (AAT), Newfoundland (Zagorevski et al. 2006). All values are recalculated to 560 Ma (DePaolo 1981).

the start of spreading (Fig. 3). Such an interpretation is consistent with the facing evidence collected by Kennedy (1971) and the absence of any detrital zircons corresponding to rift-related Neoproterozoic magmatism in the dated psammite. Cawood and Nemchin (2001) observed that late Neoproterozoic zircons occur in the rift-related units, but are generally absent in the drift-related units, probably because the rift-related magmatic rocks were largely buried as a result of thermal subsidence following the rift-drift transition.

DISCUSSION

We propose that the lithostratigraphic association of ultramafic rocks, tholeiitic gabbro, volcanic rocks and continent-derived clastic sedimentary rocks closely resembles the rock complexes found in ocean – continent transition (OCT) zones of magma-poor passive margins (see following). The ultramafic rocks in such settings mainly represent inherited sub-continental lithospheric mantle exhumed onto the seafloor and the structurally interleaved sedimentary rocks represent its syn- to post-rift cover (Manatschal 2004; Péron-Pinvidic and Manatschal 2009). The complex polyphase structural history and the relatively high pressures recorded in the mafic schist (Willner et al. 2012) are another feature typical of OCT zones, e.g. where they are preserved in ancient mountain belts such as the Alps (Beltrando et al. 2010).

Characteristics of Hyperextended Margins

Hyperextension is generally, although not exclusively, a characteristic of magma-poor margins. However, viewing margins solely on the basis of end member models is generally inappropriate, because the degree and nature of magmatism associated with hyperextension varies (e.g. Müntener and Manatschal 2006; Bernoulli et al. 2003) or may change over time from magma-poor to magma-rich (e.g. Osmundsen and Ebbing 2008). Hyperextended margins are commonly characterised by extreme thinning of parts of the continental crust (distal margin) as a result of superimposition of different modes of extension, culminating in exhumation of lowermost crust and/or serpentinized continental mantle onto the seafloor (e.g. Iberian margin; Tucholke et al. 2007; Sibuet and Tucholke 2012) and the formation of various types of thinned crustal blocks (Péron-Pinvidic and Manatschal 2010). The latter may include isolated extensional crustal allochthons riding on a concave-downwards lithosphere-scale master detachment that exhumed mantle onto the seafloor (e.g. Manatschal 2004; Manatschal et al. 2007, 2011; Sutra and Manatschal 2012). This final asymmetric phase of extension may be superimposed on an earlier phase of more symmetric extension (Huismans and Beaumont 2002) during which mantle detachments can form below both extending margins (e.g. Weinberg et al. 2007)

The exhumed, inherited mantle may be modified and refertilized by percolating melts associated with syn-rift magmatism (Müntener et al. 2009). In general, syn-rift magmatism is subdued and is represented by mafic intrusions of MORB-like composition; volcanic rocks commonly form a minor component of the mafic magmatism (but see Bernoulli et al. 2003). These mafic intrusions record the onset of magmatic accretion within the OCT zone during distributed (delocalized) extension-related deformation, which commonly continues for a significant length of time (Jagoutz et al. 2007; Péron-Pinvidic and Manatschal 2009), until the onset of true seafloor spreading and the formation of oceanic crust.

Ediacaran Hyperextension of the Humber Margin

The inferred presence in the Birchy Complex of depleted mantle rocks such as harzburgite is rare in OCT assemblages, which are generally dominated by serpentinized lherzolite. Harzburgitic mantle was locally exhumed during the Cretaceous along the Atlantic margin of Newfoundland as a result of hyperextension of the Newfoundland – Iberian sector during opening of the Atlantic Ocean. This harzburgite was interpreted as a slice of supra-subduction zone mantle inherit-

ed from a pre-Mesozoic period of subduction and melt extraction (Müntener and Manatschal 2006). Exhumation of such refractory supra-subduction zone mantle may be a mechanism that suppresses formation of syn-rift basaltic melts. Likewise, the harzburgite and dunite preserved in the Rattling Brook Group and Birchy Complex may be mantle and lower crustal cumulates of a pre-Iapetus opening phase of subduction (Grenville?). This is consistent with the trace element characteristics of the Birchy Complex mafic rocks, which exhibit MORB to backarc basin-like characteristics (Fig. 7B, C).These characteristics have been demonstrated to result from melt percolation though subduction-zone modified mantle in modern settings (e.g. Taylor 1992). Cretaceous rift-related basalts of the hyperextended Atlantic margin in offshore Newfoundland have similar characteristics (Fig. 7B), suggesting that they were derived from pre-Atlantic, Iapetan subduction-zone modified mantle (Robertson 2007). We infer a similar mechanism for the Birchy Complex suite 2 metabasites, whereby extension along the Laurentian margin leads to decompression melting of previously metasomatized mantle similar to our ultramafic rocks (Fig. 7D). Suite 1 metabasites (Fig. 7B, C) are distinctly more depleted in Th and light REE than the suite 2 metabasites and may be analogous to off-axis magmas (Reynolds and Langmuir 2000).

In addition to the ultramafic rocks in the Birchy Complex and Rattling Brook Group discussed herein, narrow slices of mantle interleaved with strongly tectonized metasedimentary rocks occur elsewhere in Newfoundland (e.g. Matthews Brook serpentinite; Cawood et al. 1996), Québec (e.g. Pennington sheet serpentinite; St. Julien 1987), and Vermont (Doolan et al. 1982), suggesting that hyperextension may have been a common process along several segments of Laurentia's Appalachian margin. There is also a close similarity between the Birchy Complex and parts of the Rattling Brook Group in Newfoundland with the upper parts (Easdale Subgroup) of the Dalradian Supergroup in western Ireland, suggesting that they occupied a similar and correlative tectonic setting (Winchester et al. 1992), directly linking the Laurentian realm of the Newfoundland Appalachians to the British Caledonides. At this stratigraphic level, best seen on southern Achill Island, serpentinite olistoliths embedded in a graphitic pelite matrix are common (Kennedy 1980; Chew 2001). The serpentinite bodies are associated with mafic volcanic rocks, deep-marine continentally derived psammitic wacke (Fig. 8), and graphitic pelite in a sequence that underwent Taconic – Grampian blueschist-facies metamorphism (Chew et al. 2003). Blueschist facies metamorphism is also preserved in correlative OCT rocks in northern Vermont (Doolan et al. 1982; Castonguay et al. 2012), emphasizing the link between high-pressure metamorphism and OCT assemblages established in the Alps (Beltrando et al. 2010) and in the Taconic – Grampian orogen of the Appalachian – Caledonian mountain belt. A discontinuous horizon of serpentinite bodies has also been documented in the Easdale Subgroup of central and northeastern Scotland (Garson and Plant 1973). The serpentinite bodies in Ireland and Scotland have been interpreted as seafloor protrusions of serpentinized mantle that were generated in Easdale Subgroup time during a phase of major crustal extension leading to the formation of an OCT (Chew 2001).

Implications of a Hyperextended Humber Margin

Evidence for Ediacaran – Early Cambrian hyperextension along segments of the Laurentian margin during opening of the Iapetus Ocean has major ramifications for understanding the evolution of the Appalachian – Caledonian margin of Laurentia in general. For example, where the sedimentary cover of rifted margins is very thick, such as the Dalradian Supergroup of the Laurentian margin in the British and Irish Caledonides (e.g. Chew 2001; Leslie et al. 2008), they may form a thermally insulating blanket; the underlying crust may therefore heat up and become rheologically weaker during rifting (Reston and Manatschal 2011). Hyperextension and the resultant formation of crustal ribbons, 'hanging wall' (H-) blocks, and extensional crustal allochthons (for definitions and characteristics of these various types of crustal blocks see Péron-Pinvidic and Manatschal 2010) are capable of explaining several puzzling and/or problematic phenomena. These include: 1) the apparent late age (525–520 Ma) of the oldest known drift sequences (e.g. Cawood et al. 2001); 2) the formation of microcontinents (e.g. Dashwoods) along the Newfoundland Humber margin and the Appalachian – Caledonian margin in general (van Staal et al. 2007, 2009b; Chew et al. 2010); 3) the markedly variable and spotty preservation of radiogenic age evidence for Taconic-related metamorphism and deformation along strike (Cawood et al. 1994; Castonguay et al. 2001, 2010 ; van Staal et al. 2009 a, b); and 4) evidence for crustal contamination in felsic rocks of the BVOT and its Early to Middle Ordovician Snooks Arm Group cover (Skulski et al. 2010) and other outboard terranes in the peri-Laurentian realm (e.g. Whalen et al. 1997; van Staal et al. 2007; Zagorevski et al. 2006)

Thermal Subsidence

The highly thinned continental margins of studied OCT zones commonly display significant retardation of thermal subsidence. In addition to the potentially insulating effects of a thick sedimentary blanket and the predicted slow cooling of the upper plate crust during asymmetric extension (Buck et al. 1988), anomalous slow cooling and prolonged uplift of a rifted margin may also be related to the structural emplacement of hot mantle under the thinning crust (Müntener et al. 2009; Péron-Pinvidic and Manatschal 2009). Hence, a combination of these processes may have significantly delayed thermal subsidence and the resultant transgression.

The time of transgression was used previously as a proxy for defining the Iapetus rift-drift transition (Bond 1984; Williams and Hiscock 1987; Cawood et al. 2001), but only provides a minimum age for break-up along this segment and probably elsewhere as well (cf. Hibbard et al. 2007). Furthermore, the work of Jagoutz et al. (2007) along the Iberian OCT has shown that formation of MORB along the proto-ridge in embryonic oceanic crust may be followed by widespread, delocalized

extensional deformation and off-axis magmatism before true spreading occurs. Therefore, the Late Neoproterozoic (565–550 Ma) eruption of MORB, backarc basin basalt (Bédard and Stevenson 1999; this paper) and other within-plate magmatism (Cawood et al. 2001; Hodych and Cox 2007) in the Newfoundland and Québec Appalachians merely places an upper limit on the onset of true seafloor spreading in this segment of the Iapetus Ocean. Spreading followed a long period (615–550 Ma) of pre-spreading, non-voluminous rift-related magmatism, exhumation of mantle onto the seafloor, and formation of embryonic (cf. Jagoutz et al. 2007) oceanic crust between 565–550 Ma (Fig. 9A). Hence, the end of rift-related magmatism (550 Ma) is the best proxy for the final breakup and onset of spreading in the Laurentian realm of the Iapetus Ocean (Fig. 9B).

Formation of Microcontinents

Microcontinents such as Dashwoods and equivalents elsewhere (e.g. Karabinos et al. 1998; Hibbard et al. 2007; van Staal and Hatcher 2010; Allen et al. 2010; Chew et al. 2008, 2010) initially could have formed, at least to a first approximation, as H-blocks or large extensional allochthons, analogous to the Briançonnais crustal block in the Alps (Manatschal et al. 2006; Mohn et al. 2010). The crust of H-blocks is commonly thinned to less than 20 km and is generally associated with marked retardation of subsidence (Péron-Pinvidic and Manatschal 2010). The characteristics of H-blocks fit the existing three dimensional seismic and petrological constraints on Dashwoods rather well (van der Velden et al. 2004; van Staal et al. 2007). Hence, we interpret Dashwoods as a microcontinent that evolved from an H-block (Fig. 9 A, B) rather than an extensional allochthon. Isotopic evidence of crustal contamination and zircon inheritance in the outboard peri-Laurentian terranes (e.g. Karabinos et al. 1998; Whalen et al. 1997; Zagorevski et al. 2006; Brem et al. 2007; Hibbard et al. 2007; van Staal et al. 2007; van Staal and Hatcher 2010; Allen et al. 2010; Chew et al. 2008, 2010; Skulski et al. 2010, Zagorevski and van Staal 2011) indicate that these isolated blocks subsequently formed the basement to supra-subduction zone magmatism in the outboard arc complexes. Formation of H-blocks and/or large extensional allochthons during hyperextension would remove the necessity of having two discrete rifting events along the Humber margin, resulting in two coeval spreading centres (Cawood et al. 2001; Waldron and van Staal 2001; Burton and Southworth 2010). This is analogous to the Briançonnais crustal block in the Alps (Manatschal et al. 2006; Mohn et al. 2010), which separates the Valais oceanic basin to the north from the Piemonte – Liguria Ocean to the south. In this analogy (Fig. 9B), the Piemonte – Liguria Ocean would represent the Iapetus Ocean and the Valais basin the Taconic seaway. However, the generation of upper plate magmatism (489–477 Ma Notre Dame arc) in Dashwoods during the closure of the Taconic seaway (van Staal et al. 2007), demands that parts of the Taconic seaway had achieved a width large enough to generate arc magmatism during its subduction beneath Dashwoods, but not so wide as to prevent exchange of Laurentian faunas. These boundary conditions suggest that the ca. 300 to1000 km wide (van Staal et al. 1998, 2007) Taconic seaway, in contrast to the Valais basin in the Alps, saw a short period (550–540 Ma) of spreading. This spreading was likely delocalized, ultra-slow and merely forming embryonic oceanic crust (Jagoutz et al. 2007); hence, the Taconic seaway was probably partially underlain by exhumed mantle and partly by oceanic lithosphere. Regardless of whether rifting and spreading was localized or delocalized, we infer that any spreading in the Taconic seaway was aborted shortly after it had started and that the dominant magmatic spreading centre formed further outboard in what would become the Iapetus Ocean (Fig. 9B), leading to separation of Dashwoods from Arequipa – Antofalla, its inferred conjugate partner (Escayola et al. 2011)

Preservation of Evidence for Taconic Deformation and Metamorphism

Other extension-related continental blocks surrounded by exhumed and serpentinized mantle, situated between Dashwoods and the autochthonous Humber margin (Fig. 9B), may explain preservation of evidence for pervasive Taconic tectono-metamorphism in these rocks compared to its apparent non-preservation in other, more inboard parts (see Cawood et al. 1994 and van Staal et al. 2009 a, b). We propose that an extensional allochthon originally formed the basement of the Rattling Brook Group east of the Bishie Cove thrust (Figs. 2, 9B, 9C). The Rattling Brook allochthon would have been subducted (abortively) beneath the BVOT and Dashwoods before arrival of the leading edge of the autochthonous Humber margin and its collision with the Notre Dame arc (van Staal et al. 2007). It follows that, because of its buoyancy, it could have returned to higher crustal levels along the subduction channel, together with the adjacent OCT zone preserved in the Birchy Complex (Fig. 9C). This may have occurred during or after the final Taconic subduction of the OCT lithosphere situated between the Rattling Brook extensional allochthon and the leading edge of the autochthonous Humber margin sitting further inboard (Fig. 9C). Such a process could have translated the Birchy Complex and spatially associated rocks to a high structural level during the Taconic orogeny (470–460 Ma), such that it remained below the Ar-closure temperature of white mica during the subsequent Salinic orogenic overprint (Cawood et al. 1994) and therefore preserved its Taconic argon ages. Although ca. 464 Ma metamorphic zircon in retrogressed eclogite pods leaves little doubt that the autochthonous Humber margin was subjected to Taconic burial as well (van Staal et al. 2009 a, b), Taconic argon ages are typically not preserved in the adjacent rocks (Hibbard, 1983). This is likely because the autochthonous Humber margin was in many places subjected to significant Silurian (Salinic) tectonic burial and resetting. In this model, the serpentinites along the Bishie Cove thrust would thus define a suture between para-authochthonous Humber margin rocks and allochthonous OCT lithosphere attached to the Rattling Brook allochthon positioned further outboard (Fig. 9C). Chew et al. (2010) proposed a rather similar model for the

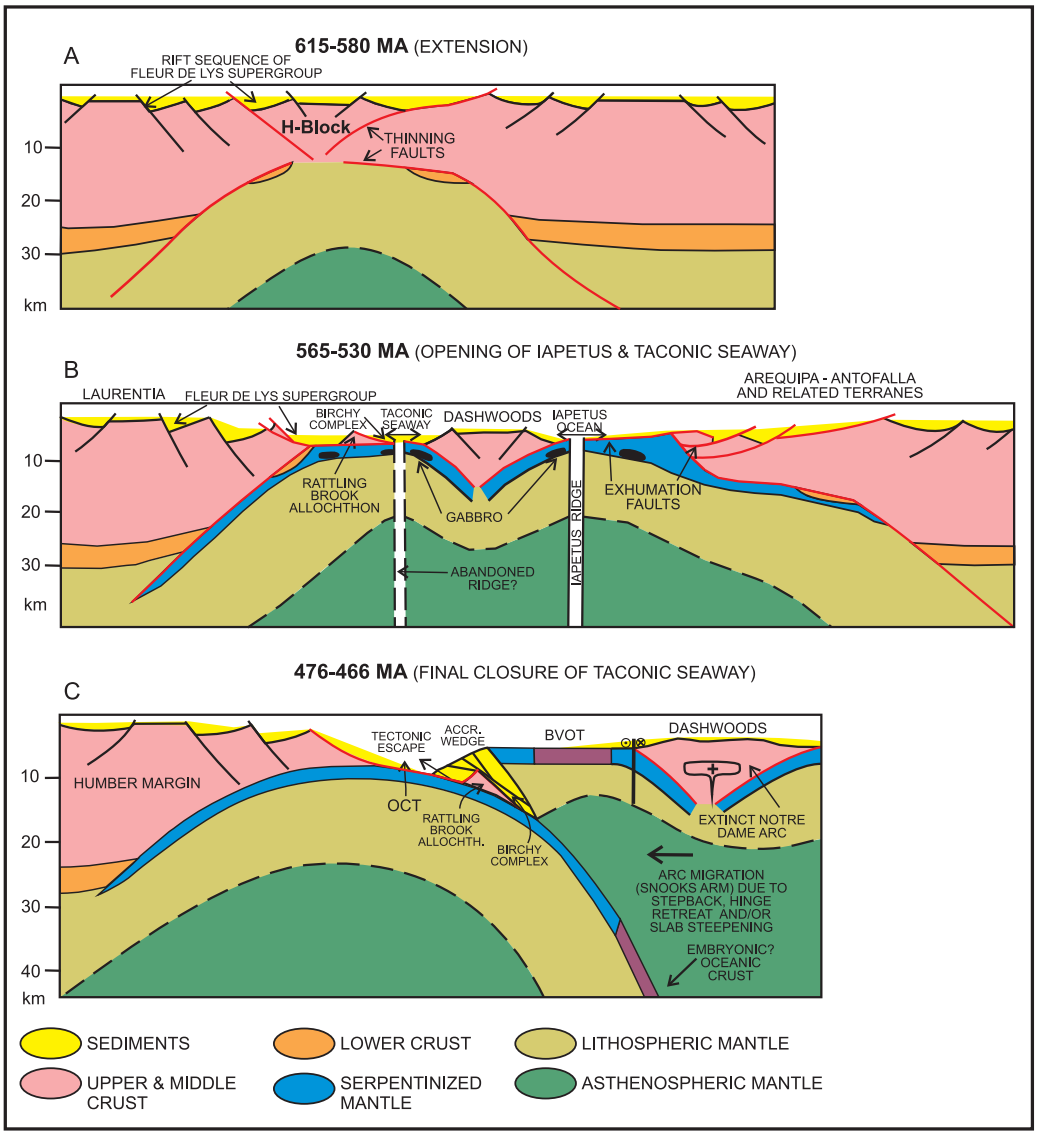

Figure 9. Schematic tectonic evolution of the hyperextended segment of the Humber margin, preserved on the Baie Verte peninsula of northwestern Newfoundland. A. Extensional structures formed during the early stages of rifting (615–580 Ma). It is inferred that Dashwoods started out as a keystone between conjugate normal faults (hanging wall block) associated with thinning of the lithosphere. This part of the model follows the structural evolution proposed by Mohn et al. (2010) for the isolation of the Briançonnais block through formation of the Valais and Ligurian – Piemonte oceanic seaways in the Alpine Tethys. B. Isolation of Dashwoods as a microcontinent following development of large detachment faults, which exhumed mantle onto the seafloor on both sides. The Rattling Brook block forms as a major extensional allochthon that was separated from the authochthonous Humber margin by exhumed mantle and overlain by sediments of the Fleur de Lys Supergroup. Extension and separation of the Rattling Brook allochthon from the Humber margin continued until the onset of spreading in the Taconic seaway between 550 and 540 Ma. This spreading is necessary to form an oceanic basin wide enough to generate Early Ordovician arc magmatism in Dashwoods and above the Baie Verte oceanic tract (BVOT) during its closure. Spreading subsequently jumped outboard of Dashwoods between 540 and 530 Ma, opening the Iapetus Ocean and separating Dashwoods from its conjugate margin, which is assumed to be the Arequipa – Antofalla ribbon continent and related terranes (Escayola et al. 2011). C. Final closure of the Taconic seaway by east-directed subduction, which culminated in Taconic orogenesis. East-directed subduction began in the Taconic seaway at ca. 490 Ma, forming the 490–483 Ma supra-subduction zone BVOT (van Staal et al. 2007, 2009b). The latter subsequently became the forearc terrane to the 489–477 Ma Notre Dame arc, as indicated by ample continental arc fragments in the basal part of the Flat Water Pond/Snooks Arm Group (Bédard et al. 2000; Skulski et al. 2010). Earlier west-directed subduction within the Taconic seaway may have started during the Middle Cambrian, culminating in obduction of the Lushes Bight oceanic tract onto Dashwoods and subduction polarity reversal (see Zagorevski and van Staal 2011), but is not shown here for the sake of simplicity. Partial subduction of the Rattling Brook allochthon at ca. 479 Ma is thought to be the cause of the extinction of the Notre Dame arc in Dashwoods by ca. 477 Ma. Convergence continued through subduction of the segment of the Taconic seaway mainly underlain by serpentinized mantle that separated the (para) autochthonous Humber margin from the Rattling Brook allochthon. Hinge retreat and possibly steepening of the downgoing slab may explain the west-directed migration of upper plate arc-backarc magmatism from Dashwoods onto the BVOT, forming the 479–467 Ma Flat Water Pond/Snooks Arm Group, which forms a disconformable cover sequence to the BVOT (Skulski et al. 2010).

Grampian in the west of Ireland. In addition, slow but relatively steep subduction of the OCT lithosphere (partly serpentinized mantle?) between the Humber margin and the Rattling Brook allochthon, beneath the BVOT, could be responsible for generating the arc – backarc-like magmatism preserved in the Flat Water Pond/Snooks Arm Group, which disconformably covers the BVOT (Skulski et al. 2010).

CONCLUSION

The extent of hyperextension along the Laurentian margin is difficult to assess at present, but the evidence of detached peri-Laurentian blocks having been subjected to different tectonic evolutions during the Taconic – Grampian orogen is widespread (e.g. Karabinos et al.1998; Hibbard et al. 2007; van Staal et al. 2007; van Staal and Hatcher 2010; Leslie et al. 2008; Chew et al. 2008, 2010; Allen et al. 2010). Laurentia's Appalachian – Caledonian margin may therefore have been characterised by large, magma-poor, hyperextended segments.

Considering the poor age constraints on the timing of the rift-drift transition, it is difficult to assess the overall sense of diachroneity in the opening of the Iapetus Ocean. However, available data suggest that rifting progressed from northeast to southwest in present coordinates, being the oldest in Baltica (Bingen et al. 1998) and becoming younger in Scotland (e.g. Leslie et al. 2008) and the Appalachians (van Staal et al. 1998; Cawood et al. 2001; Burton and Southworth 2010).

The reason for Late Cambrian (495–490 Ma) subduction initiation in the Taconic seaway in Newfoundland (van Staal et al. 1998, 2007) and near the Grampian margin in the west of Ireland (Chew et al. 2010), rather than in the outboard Iapetus, remains elusive. Numerical analysis has shown that initiating subduction in old and cold oceanic lithosphere near a continental margin is very difficult, because the strength of such lithosphere is higher than the forces that drive subduction (e.g. Cloetingh et al. 1989), although potential exceptions under special conditions have been proposed (Nikolaeva et al. 2011). However, as indicated by Beltrando et al. (2010) and Reston and Manatschal (2011), the serpentinite shear zones formed during extension represent major zones of weakness, which could have facilitated initiation of subduction following the onset of compression during the Middle Cambrian in the Iapetus Ocean (van Staal and Hatcher 2010) and Taconic seaway (Zagorevski and van Staal 2011). Regardless of whether this is correct, the earliest rifting history along the Laurentian margin likely had a profound impact on the closure of Iapetan seaways and generation of associated arc magmatism in the Laurentian realm.

ACKNOWLEDGEMENTS

This is a contribution to the Targeted Geoscience Intiative program, (2000–2015; GSC contribution #20120367). Discussions with Jean Bédard, Hank Williams and Andy Kerr were helpful in enhancing our understanding of Baie Verte geology. We are grateful for the comments by reviewers Paul Karabinos and Gianreto Manatschal, which improved the manuscript. The first author (CvS) especially would like to thank Paul Hoffman for an enduring friendship and the numerous, very inspiring weekly discussions on all aspects of geology, particularly tectonics, during the first 6 years of his tenure at the GSC. The discussions lasted often late into the night or early morning, commonly becoming progressively more interesting and vocal following progressive consumption of alcohol.

REFERENCES

Allen, J.S., Thomas, W.A., and Lavoie, D., 2010, The Laurentian margin of northeastern North America, *in* Tollo, R.P., Batholomew, M.J., Hibbard, J.P., and Karabinos, P.M., *eds.*, From Rodinia to Pangea: The lithotectonic record of the Appalachian region: Geological Society of America Memoir, 206, p. 71–90, http://dx.doi.org/10.1130/2010.1206(04).

Bédard, J.H., and Escayola, M., 2010, The Advocate ophiolite mantle, Baie Verte, Newfoundland: regional correlations and evidence for metasomatism: Canadian Journal of Earth Sciences, v. 47, p. 237–253, http://dx.doi.org/10.1139/E10-004.

Bédard, J.H., and Stevenson, R., 1999, The Caldwell Group lavas of southern Quebec: MORB-like tholeiites associated with the opening of Iapetus Ocean: Canadian Journal of Earth Sciences, v. 36, p. 999–1019, http://dx.doi.org/10.1139/e99-018.

Bédard, J.H., Lauziere, K., Tremblay, A., Sangster, A., Douma, S.L., and Dec, T., 2000, Betts Cove ophiolite and its cover rocks, Newfoundland: Geological Survey of Canada, Bulletin 550, 76 p.

Beltrando, M., Rubatto, D., and Manatschal, G., 2010, From passive margins to orogens: The link between ocean-continent transition zones and (ultra) high-pressure metamorphism: Geology, v. 38, p. 559–562, http://dx.doi.org/10.1130/G30768.1.

Bernoulli, D., Manatschal, G., Desmurs, L., and Müntener, O., 2003, Where did Gustav Steinmann see the trinity? Back to the roots of an Alpine ophiolite concept, *in* Dilek, Y., and Newcomb, S., *eds.*, Ophiolite concept and the evolution of geological thought: Geological Society of America Special Paper 373, p 93–110, http://dx.doi.org/10.1130/0-8137-2373-6.93.

Bingen, B., Demaiffe, D., and van Breemen, O., 1998, The 616 Ma Old Egersund Basaltic Dike Swarm, SW Norway, and Late Neoproterozoic opening of the Iapetus Ocean: The Journal of Geology, v. 106, p. 565–574, http://dx.doi.org/10.1086/516042.

Bond, G.C., Nickeson, P.A., and Kominz, M.A., 1984, Breakup of a supercontinent between 625 Ma and 555 Ma: new evidence and implications for continental histories: Earth and Planetary Science Letters, v. 70, p. 325–345, http://dx.doi.org/10.1016/0012-821X(84)90017-7.

Brem, A.G., Lin, S. van Staal, C.R, Davis, D.W., and McNicoll, V.J., 2007, The Middle Ordovician to Early Silurian voyage of the Dashwoods microcontinent, West Newfoundland, based on new U/Pb and $^{40}Ar/^{39}Ar$ geochronological, and kinematic constraints: American Journal of Science, v. 307, p. 311–338, http://dx.doi.org/10.2475/02.2007.01.

Buck, W.R., Martinez, F., Steckler, M.S., and Cochran, J.R., 1988, Thermal consequences of lithospheric extension: Pure and simple: Tectonics, v. 7, p. 213–234, http://dx.doi.org/10.1029/TC007i002p00213.

Bursnall, J.T., 1975, Stratigraphy, structure and metamorphism west of Baie Verte, Burlington Peninsula, Newfoundland: Unpublished PhD thesis, Cambridge University, England, 337 p.

Bursnall, J.T., and de Wit, M.J., 1975, Timing and development of the orthotectonic zone in the Appalachian orogen of northwest Newfoundland: Canadian Journal of Earth Sciences, v. 12, p. 1712–1722, http://dx.doi.org/10.1139/e75-152.

Burton, W.C., and Southworth, S., 2010, A model for Iapetan rifting of Laurentia based on Neoproterozoic dikes and related rocks, *in* Tollo, R.P., Batholomew, M.J., Hibbard, J.P., and Karabinos, P.M., *eds.*, From Rodinia to Pangea: The lithotectonic record of the Appalachian region: Geological Society of America Memoir 206, p. 455–476.

Cabanis, B., and Lecolle, M., 1989, Le diagramme La/10-Y/15-Nb/8; un outil pour la discrimination des series volcaniques et la mise en evidence des processus de melange et/ou de contamination crustale. The La/10–Y/15–Nb/8 diagram; A tool for distinguishing volcanic series and discovering crustal mixing and/or contamination: Comptes Rendus de l'Academie des Sciences, Serie 2, Mecanique, Physique, Chimie, Sciences de l'Univers, Sciences de la Terre, v. 309, p. 2023–2029.

Castonguay, S., Ruffet, G., Tremblay, A., and Féraud, G., 2001, Tectonometamorphic evolution of the southern Quebec Appalachians: $^{40}Ar/^{39}Ar$ evidence for Middle Ordovician crustal thickening and Silurian–Early Devonian exhumation of the internal Humber zone: Geological Society of America Bulletin, v. 113, p. 144–160, http://dx.doi.org/10.1130/0016-7606(2001)113<0144:TEOTSQ>2.0.CO;2.

Castonguay, S., Skulski, T., van Staal, C.R., McNicoll, V., and Joyce, N., 2010, Structure and timing of deformation and metamorphism of the Baie Verte Peninsula, Newfoundland Appalachians, *in* Kerr, A. and Pereira, C., *eds.*, Annual Meeting Geological Association of Canada: Newfoundland and Labrador section Program and Abstracts, p.2.

Castonguay, S., Kim, J., Thompson, P.J., Gale, M.H., Joyce, N., Laird, J., and Doolan, B.L., 2012, Timing of tectonometamorphism across the Green Mountain anticlinorium, northern Vermont Appalachians: $^{40}Ar/^{39}Ar$ data and correlations with southern Quebec: Geological Society of America Bulletin, v. 124, p. 352–367, http://dx.doi.org/10.1130/B30487.1.

Cawood, P.A., and Nemchin, A.A., 2001, Paleogeographic development of the east Laurentian margin: Constraints from U–Pb dating of detrital zircons in the Newfoundland Appalachians: Geological Society of America Bulletin, v. 113, p. 1234–1246, http://dx.doi.org/10.1130/0016-7606(2001)113<1234:PDOTEL>2.0.CO;2.

Cawood, P.A., Dunning, G.R., Lux, D., and van Gool, J.A.M., 1994, Timing of peak metamorphism and deformation along the Appalachian margin of Laurentia in Newfoundland: Silurian, not Ordovician: Geology, v. 22, p. 399–402, http://dx.doi.org/10.1130/0091-7613(1994)022<0399:TOPMAD>2.3.CO;2.

Cawood, P.A., van Gool, J.A.M., and Dunning, G.R., 1996, Geological development of eastern Humber and western Dunnage zones: Corner Brook – Glover Island region, Newfoundland: Canadian Journal of Earth Sciences, v. 33, p. 182–198, http://dx.doi.org/10.1139/e96-017.

Cawood, P.A., McCausland, P.J.A., and Dunning, G.R., 2001, Opening Iapetus: Constraints from the Laurentian margin in Newfoundland: Geological Society of America Bulletin, v. 113, p. 443–453, http://dx.doi.org/10.1130/0016-7606(2001)113<0443:OICFTL>2.0.CO;2.

Chew, D.M., 2001, Basement protrusion origin of serpentinite in the Dalradian: Irish Journal of Earth Sciences, v. 19, p. 23–35.

Chew, D.M., 2003, Structural and stratigraphic relationships across the continuation of the Highland Boundary Fault in western Ireland: Geological Magazine, v. 140, p. 73–85, http://dx.doi.org/10.1017/S0016756802007008.

Chew, D.M., Daly, J.S., Page, L.M., and Kennedy, M.J., 2003, Grampian orogenesis and the development of blueschist-facies metamorphism in western Ireland: Journal of the Geological Society, v. 160, p. 911–924, http://dx.doi.org/10.1144/0016-764903-012.

Chew, D.M., Flowerdew, M.J., Page, L.M., Crowley, Q.G., Daly, J.S., Cooper, M., and Whitehouse, M.J., 2008, The tectonothermal evolution and provenance of the Tyrone Central Inlier, Ireland: Grampian imbrication of an outboard Laurentian microcontinent?: Journal of the Geological Society, v. 165, p. 675–685, http://dx.doi.org/10.1144/0016-76492007-120.

Chew, D.M., Daly, J.S., Magna, T., Page, L.M., Kirkland, C.L., Whitehouse, M.J., and Lam, R., 2010, Timing of ophiolite obduction in the Grampian orogen: Geological Society of America Bulletin, v. 122, p. 1787–1799, http://dx.doi.org/10.1130/B30139.1.

Cloetingh, S., Wortel, R., and Vlaar, N.J., 1989, On the initiation of subduction zones: Pure and Applied Geophysics, v. 129, p. 7–25, http://dx.doi.org/10.1007/BF00874622.

De Paolo, D.J., 1981, Neodymium isotopes in the Colorado Front Range and crust–mantle evolution in the Proterozoic: Nature, v. 291, p. 193–196, http://dx.doi.org/10.1038/291193a0.

de Wit , M.J., and Strong, D.F., 1975, Eclogite-bearing amphibolites from the Appalachian mobile belt, northwest Newfoundland: Dry versus wet metamorphism: The Journal of Geology, v. 83, p. 609–627, http://dx.doi.org/10.1086/628144.

Doolan, B.L., Gale, M.H., Gale, P.N., and Hoar, R.S., 1982, Geology of the Quebec Re-entrant: Possible constraints from early rifts and the Vermont-Quebec serpentinite belt, *in* St. Julien, P., and Beland, J., *eds.*, Major structural zones and faults of the northern Appalachians: Geological Association of Canada Special Paper 24, p. 87–116.

Dunning, G.R., and Krogh, T.E., 1985, Geochronology of ophiolites of the Newfoundland Appalachians: Canadian Journal of Earth Sciences, v. 22, p. 1659–1670, http://dx.doi.org/10.1139/e85-174.

Escayola, M.P., van Staal, C.R., and Davis, W.J., 2011, The age and tectonic setting of the Puncoviscana Formation in northwestern Argentina: An accretionary complex related to Early Cambrian closure of the Puncoviscana Ocean and accretion of the Arequipa-Antofalla block: Journal of South American Earth Sciences, v. 32, p. 438–459, http://dx.doi.org/10.1016/j.jsames.2011.04.013.

Garson, M.S., and Plant, J., 1973, Alpine type ultramafic rocks and episodic mountain building in the Scottish Highlands: Nature Physical Science, v. 242, p. 34–38, http://dx.doi.org/10.1038/physci242034a0.

Gower, C.F., Kamo, S.L., Kwok, K., and Krogh, T.E., 2008, Proterozoic southward accretion and Grenvillian orogenesis in the interior Grenville Province in eastern Labrador: Evidence from U–Pb geochronological investigations: Precambrian Research, v. 165, p. 61–95, http://dx.doi.org/10.1016/j.precamres.2008.06.007.

Heaman, L.M., Erdmer, P., and Owen, J.V., 2002, U–Pb geochronologic con-

straints on the crustal evolution of the Long Range Inlier, Newfoundland: Canadian Journal of Earth Sciences, v. 39, p. 845–865, http://dx.doi.org/10.1139/e02-015.

Hibbard, J., 1983, Geology of the Baie Verte Peninsula, Newfoundland: Mineral Development division Department of Mines and Energy, Government of Newfoundland and Labrador, Memoir 2, 279 p.

Hibbard, J., 1988, Stratigraphy of the Fleur de Lys Belt, northwest Newfoundland, *in* Winchester, J.A., *ed.*, Later Proterozoic Stratigraphy of the Northern Atlantic Regions: Springer, US, p. 200–211, http://dx.doi.org/10.1007/978-1-4615-7344-9_16.

Hibbard, J.P., St. Julien, P., and Trzcienski, W.E., Jr., 1995, Humber Zone internal, *in* Williams, H., *ed.,* Chapter 3 of Geology of the Appalachian-Caledonian Orogen in Canada and Greenland: Geological Survey of Canada, Geology of Canada, no. 6, p. 114–139.

Hibbard, J.P., van Staal, C.R., and Rankin, D.W., 2007, A comparative analysis of pre-Silurian crustal building blocks of the northern and the southern Appalachian orogen: American Journal of Science, v. 307, p. 23–45, http://dx.doi.org/10.2475/01.2007.02.

Hodych, J.P., and Cox, R.A., 2007, Edicaran U–Pb zircon dates for the Lac Matapedia and Mt. St.-Anselme basalts of the Quebec Appalachians: support for a long-lived mantle plume during the rifting phase of Iapetus opening: Canadian Journal of Earth Sciences, v. 44, p. 565–581, http://dx.doi.org/10.1139/e06-112.

Huismans, R.S., and Beaumont, C., 2002, Asymmetric lithospheric extension: The role of frictional plastic strain softening inferred from numerical experiments: Geology, v. 30, p. 211–214, http://dx.doi.org/10.1130/0091-7613(2002)030<0211:ALETRO>2.0.CO;2.

Jaffey, A.H., Flynn, K.F., Glendenin, L.E., Bentley, W.C., and Essling, A.M., 1971, Precision measurement of half-lives and specific activities of ^{235}U and ^{238}U: Physical Review C, v. 4, p. 1889–1906, http://dx.doi.org/10.1103/PhysRevC.4.1889.

Jagoutz, O., Müntener, O., Manatschal, G., Rubatto, D., Péron-Pinvidic, G., Turrin, B.D., and Villa, I.M., 2007, The rift-to-drift transition in the North Atlantic: A stuttering start of the MORB machine?: Geology, v. 35, p. 1087–1090, http://dx.doi.org/10.1130/G23613A.1.

Kamo, S.L., Gower, C.F., and Krogh, T.E., 1989, Birthdate for the Iapetus Ocean? A precise U–Pb zircon and baddeleyite age for the Long Range dikes, southeast Labrador: Geology, v. 17, p. 602–605, http://dx.doi.org/10.1130/0091-7613(1989)017<0602:BFTLOA>2.3.CO;2.

Karabinos, P., Samson, S.D., Hepburn, J.C., and Stoll, H.M., 1998, Taconian orogeny in the New England Appalachians: Collision between Laurentia and the Shelburne Falls arc: Geology, v. 26, p. 215–218, http://dx.doi.org/10.1130/0091-7613(1998)026<0215:TOITNE>2.3.CO;2.

Kennedy, M.J., 1971, Structure and stratigraphy of the Fleur de Lys Supergroup in the Fleur de Lys area, Burlington Peninsula, Newfoundland: Geological Association of Canada, Proceedings 24, p. 59–71.

Kennedy, M.J., 1980, Serpentinite-bearing melange in the Dalradian of County Mayo and its significance in the development of the Dalradian Basin: Journal of Earth Sciences, Royal Dublin Society, v. 3, p. 117-126.

Košler, J., and Sylvester, P.J., 2003, Present trends and the future of zircon in geochronology: Laser ablation ICPMS: Reviews in Mineralogy and Geochemistry, v. 53, p. 243–275, http://dx.doi.org/10.2113/0530243.

Košler, J., Forst, L., Sláma, J., 2008, Lamdate and Lamtool: spreadsheet-based data reduction for laser ablation ICP-MS, *in* Sylvester, P., *ed.*, Laser Ablation ICP-MS in the Earth Sciences: Current Practices and Outstanding Issues: Mineralogical Association of Canada, Short Course Series 40, p. 315-317.

Krogh, T.E., 1982, Improved accuracy of U–Pb zircon ages by the creation of more concordant systems using an air abrasion technique: Geochimica et Cosmochimica Acta, v. 46, p. 637–649, http://dx.doi.org/10.1016/0016-7037(82)90165-X.

Kumarapeli, P.S., Dunning, G.R., Pintson, H., and Shaver, J., 1989, Geochemistry and U–Pb zircon age of comenditic metafelsites of the Tibbit Hill Formation, Quebec Appalachians: Canadian Journal of Earth Sciences, v. 26, p. 1374–1383, http://dx.doi.org/10.1139/e89-117.

Leslie, A G., Smith, M., and Soper, N.J., 2008, Laurentian margin evolution and the Caledonian orogeny – A template for Scotland and East Greenland, *in* Higgins, A.K., Giulotti, J.A., and Smith, M.P., *eds.*, The Greenland Caledonides: Evolution of the Northeast margin of Laurentia: Geological Society of America Memoir 202, p. 307–343, http://dx.doi.org/10.1130/2008.1202(13).

Ludwig, K.R., 2003, User's manual for Isoplot/Ex rev.3.00: A geochronological Toolkit for Microsoft Excel, v. 4: Berkeley Geochronology Center Special Publication, Berkeley, California, U.S.A., p. 1–70.

Manatschal, G., 2004, New models for evolution of magma-poor rifted margins based on a review of data and concepts from West Iberia and the Alps: International Journal of Earth Sciences, v. 93, p. 432–466, http://dx.doi.org/10.1007/s00531-004-0394-7.

Manatschal, G., and Müntener, O., 2009, A type sequence across an ancient magma-poor ocean-continent transition: the example of the western Alpine Tethys ophiolites: Tectonophysics, v. 473, p. 4–19, http://dx.doi.org/10.1016/j.tecto.2008.07.021.

Manatschal, G., Engström, A., Desmurs, L., Schaltegger, U., Cosca, M., Müntener, O., Bernoulli, D., 2006, What is the tectono-metamorphic evolution of continental break-up: The example of the Tasna Ocean-Continent transition: Journal of Structural Geology, v. 28, p. 1849–1869, http://dx.doi.org/10.1016/j.jsg.2006.07.014.

Manatschal, G., Müntener, O., Lavier, L.L, Minshull, T. A., and Péron-Pinvidic, G., 2007, Observations from the alpine Tethys and Iberia-Newfoundland margins pertinent to the interpretation of continental breakup, *in* Karner, G.D., Manatschal, G., and Pinheiro, L.M., *eds.*, Imaging, Mapping and Modeling Continental Lithosphere Extension and Breakup: Geological Society, London, Special Publications 282, p. 291–324.

Manatschal, G., Sauter, D., Karpoff, A.M., Masini, E., Mohn, G., and Lagabrielle, Y., 2011, The Chenaillet Ophiolite in the French/Italian Alps: An ancient analogue for an oceanic core complex?: Lithos, v. 124, p. 169–184, http://dx.doi.org/10.1016/j.lithos.2010.10.017.

McCausland, P.J.A., Van der Voo, R., and Hall, C.M., 2007, Circum-Iapetus paleogeography of the Precambrian-Cambrian transition with a new paleomagnetic constraint from Laurentia: Precambrian Research, v. 156, p. 125–152, http://dx.doi.org/10.1016/j.precamres.2007.03.004.

Mitchell, R.N., Kilian, T.M., Raub, T.D., Evans, D.A.D, Bleeker, W., and Mal-

oof, A.C., 2011, Sutton hotspot: Resolving Ediacaran-Cambrian tectonics and true polar wander for Laurentia: American Journal of Science, v. 311, p. 651–663, http://dx.doi.org/10.2475/08.2011.01.

Mohn, G., Manatschal, G., Müntener, O., Beltrando, M., and Masini, E., 2010, Unravelling the interaction between tectonic and sedimentary processes during lithospheric thinning in the Alpine Tethys margins: International Journal of Earth Sciences, v. 99, p. 75–101, http://dx.doi.org/10.1007/s00531-010-0566-6.

Müntener, O., and Manatschal, G., 2006, High degrees of melt extraction recorded by spinel harzburgite of the Newfoundland margin: The role of inheritance and consequences for the evolution of the southern North Atlantic: Earth and Planetary Science Letters, v. 252, p. 437–452, http://dx.doi.org/10.1016/j.epsl.2006.10.009.

Müntener, O., Manatschal, G., Desmurs, L., and Pettke, T., 2009, Plagioclase peridotites in Ocean-continent transitions: Refertilised mantle domains generated by melt stagnation in the shallow mantle lithosphere: Journal of Petrology, v. 51, p. 153–183.

Nikolaeva, K., Gerya, T.V., and Marques, F.O., 2011, Numerical analysis of subduction initiation risk along the Atlantic American passive margins: Geology, v. 39, p. 463–466, http://dx.doi.org/10.1130/G31972.1.

Niu, Y., 2004, Bulk-rock major and trace element compositions of abyssal peridotites: Implications for mantle melting, melt extraction and post-melting processes beneath mid-ocean ridges: Journal of Petrology, v. 45(12), p. 2423–2458, http://dx.doi.org/10.1093/petrology/egh068.

O'Brien, T.M., and van der Pluijm, B.A., 2012, Timing of Iapetus Ocean rifting from Ar geochronology of pseudotachylytes in the St. Lawrence rift system of southern Quebec: Geology, v. 40, p. 443–446, http://dx.doi.org/10.1130/G32691.1.

Osmundsen, P.T., and Ebbing, J., 2008, Styles of extension offshore mid-Norway and implications for mechanisms of crustal thinning at passive margins: Tectonics, v. 27, TC6016, http://dx.doi.org/10.1029/2007TC002242.

Parrish, R.R., Roddick, J.C., Loveridge, W.D., and Sullivan, R.W., 1987, Uranium–lead analytical techniques at the geochronology laboratory: Geological Survey of Canada Paper 87-2, p. 3–7.

Pearce, J.A., 1996, A user's guide to basalt discrimination diagrams, *in* Wyman, D.A., *ed.,* Trace element geochemistry of volcanic rocks: Applications for massive sulphide exploration: Geological Association of Canada, Short Course Notes, v. 12, p. 79–113.

Pearce, J.A., Harris, N.B.W., and Tindle, A.G., 1984, Trace element discrimination diagrams for the tectonic interpretation of granitic rocks: Journal of Petrology, v. 25, p. 956–983, http://dx.doi.org/10.1093/petrology/25.4.956.

Péron-Pinvidic, G., and Manatschal, G., 2009, The final rifting evolution at a deep magma-poor passive margins from Iberia-Newfoundland: A new point of view: International Journal of Earth Sciences, v. 98, p. 1581–1597, http://dx.doi.org/10.1007/s00531-008-0337-9.

Péron-Pinvidic, G., and Manatschal, G., 2010, From microcontinents to extensional allochthons: witnesses of how continents rift and break apart?: Petroleum Geoscience, v. 16, p. 189–197, http://dx.doi.org/10.1144/1354-079309-903.

Pollock, J.C., Hibbard, J.P., and Sylvester, P.J., 2009, Early Ordovician rifting of Avalonia and birth of the Rheic Ocean: U–Pb detrital zircon constraints from Newfoundland: Journal of the Geological Society, v. 166, p. 501–515, http://dx.doi.org/10.1144/0016-76492008-088.

Puffer, J.H., 2002, A late Neoproterozoic eastern Laurentia superplume: Location, size, chemical composition, and environmental impact: American Journal of Science, v. 302, p. 1–27, http://dx.doi.org/10.2475/ajs.302.1.1.

Reston, T., and Manatschal, G., 2011, Rifted margins: Building blocks of later collision- Chapter 1, *in* Brown, D., and Ryan, P.D., *eds*, Arc-Continent Collision, Frontiers in Earth Sciences: Springer Verlag, Berlin Heidelberg, p. 3–21, http://dx.doi.org/10.1007/978-3-540-88558-0_1.

Reynolds., J.R., and Langmuir, C.H., 2000, Identification and implications of off-axis lava flows around the east Pacific Rise: Geochemistry, Geophysics, Geosystems, v. 1, 1999GC000033.

Richard, P., Shimizu, N., and Allègre, C.J., 1976, $^{143}Nd/^{146}Nd$, a natural tracer: an application to oceanic basalts: Earth and Planetary Science Letters, v. 31, p. 269–278, http://dx.doi.org/10.1016/0012-821X(76)90219-3.

Robertson, A.H.F., 2007, Evidence of continental breakup from the Newfoundland rifted margin (Ocean Drilling Program Leg 210): Lower Cretaceous seafloor formed by exhumation of subcontinental mantle lithosphere, and the transition to seafloor spreading, *in* Tucholke, B.E., Sibuet, J.-C., and Klaus, A., *eds.*, Proceedings of the Ocean Drilling Program, Scientific Results, v. 210: College Station, TX (Ocean Drilling Program), p. 1–69, http://dx.doi.org/10.2973/odp.proc.sr.210.104.2007.

Roddick, J.C., 1987, Generalized numerical error analysis with applications to geochronology and thermodynamics: Geochimica et Cosmochimica Acta, v. 51, p. 2129–2135, http://dx.doi.org/10.1016/0016-7037(87)90261-4.

Savov, I.P., Ryan, J.G., D'Antonio, M., Kelley, K., and Mattie, P., 2005, Geochemistry of serpentinized peridotites from the Mariana forearc Conical Seamount, ODP Leg 125: Implications for the elemental recycling at subduction zones: Geochemistry, Geophysics, Geosystems, v. 6, Q04J15, http://dx.doi.org/10.1029/2004GC000777.

Sibuet, J.C., and Tucholke, B.E., 2012, The geodynamic province of transitional lithosphere adjacent to magma-poor continental margins: Geological Society of London Special Publications 369, http://dx.doi.org/10.1144/SP369.15.

Skulski, T., Castonguay, S., McNicoll, V., van Staal, C.R., Kidd, W., Rogers, N., Morris, W., Ugalde, H., Slavinski, H., Spicer, W., Moussalam, Y., and Kerr, I., 2010, Tectonostratigraphy of the Baie Verte oceanic tract and its ophiolite cover sequence on the Baie Verte peninsula: Current Research, Newfoundland and Labrador Department of Natural Resources, Geological Survey Report 10-1, p. 315–335.

Sláma, J., Košler, J., Condon, D.J., Crowley, J.L., Gerdes, A., Hanchar, J.M., Horstwood, M.S.A., Morris, G.A., Nasdala, L., Norberg, N., Schaltegger, U., Schoene, B., Tubrett, M.N. and Whitehouse, M.J., 2008, Plešovice zircon – A new natural reference material for U–Pb and Hf isotopic microanalysis: Chemical Geology, v. 249, p. 1–35, http://dx.doi.org/10.1016/j.chemgeo.2007.11.005.

St.-Julien, P., 1987, Géologie des régions de St. Victor et de Thetford mines (moitié est): Ministère de l'Énergie et des Ressources du Québec Report MM 8601, 66 p.

Stacey, J.S., Kramers, J.D., 1975, Approximation of terrestrial lead isotope evolution by a two-stage model: Earth and Planetary Science Letters, v. 26,

p.207–221, http://dx.doi.org/10.1016/0012-821X(75)90088-6.

Sun, S.-s., and McDonough, W.F., 1989, Chemical and isotopic systematics of oceanic basalts: Implications for mantle composition and processes: Geological Society, London Special Publications, v. 42, p. 313–345, http://dx.doi.org/10.1144/GSL.SP.1989.042.01.19.

Sutra, E., and Manatschal, G., 2012, How does the continental crust thin in a hyperextended rifted margin? Insights from the Iberia margin: Geology, v. 40, p. 139–142, http://dx.doi.org/10.1130/G32786.1.

Sylvester, P.J., and Ghaderi, M., 1997, Trace element analysis of scheelite by excimer laser ablation-inductively coupled plasma-mass spectrometry (ELA-ICP-MS) using a synthetic glass standard: Chemical Geology, v. 141, p. 49–65, http://dx.doi.org/10.1016/S0009-2541(97)00057-0.

Taylor, B., 1992, Rifting and the volcanic-tectonic evolution of the Izu-Bonin-Mariana Arc, *in* Taylor, B., Fujioka, K. et al., *eds.,* Proceedings of the Ocean Drilling Program, Scientific Results, v. 126, p. 627–651.

Tollo, R.P., Aleinikoff, J.N., Bartholomew, M.J, and Rankin, D.W., 2004, Neoproterozoic A-type granitoids of the central and southern Appalachians: intraplate magmatism associated with episodic rifting of the Rodinian supercontinent: Precambrian Research, v. 128, p. 3–38, http://dx.doi.org/10.1016/j.precamres.2003.08.007.

Tucholke, B.E., Sawyer, D.S., and Sibuet, J.C., 2007, Break-up of the Newfoundland-Iberia rift, *in* Karner, G.D., Manatschal, G., and Pinheiro, L.M., *eds.*, Imaging, Mapping and Modelling Continental Lithosphere Extension and breakup: Geological Society Special Publications 282, p. 9–46.

van der Velden, A.J., van Staal, C.R., and Cook, F.A., 2004, Crustal structure, fossil subduction, and the tectonic evolution of the Newfoundland Appalachians: Evidence from a reprocessed seismic reflection survey: Geological Society of America Bulletin, v. 116, p. 1485-1498, http://dx.doi.org/10.1130/B25518.1.

van Staal, C.R., and Hatcher, R.D, Jr., 2010, Global setting of Ordovician orogenesis, *in* Finney, S., Barnes, C., and Berry, R., *eds.*, Global Ordovician earth systems: Geological Society of America Special Paper 466, p. 1–11, http://dx.doi.org/10.1130/2010.2466(01).

van Staal, C.R., Dewey, J.F., MacNiocaill, C., and McKerrow, S., 1998, The Cambrian–Silurian tectonic evolution of the northern Appalachians: History of a complex, southwest Pacific-type segment of Iapetus, *in* Blundell, D.J., and Scott, A.C., *eds.*, Lyell: The Past is the Key to the Present: Geological Society Special Publication 143, p. 199–242.

van Staal, C.R., Whalen, J.B., McNicoll, V.J., Pehrsson, S.J., Lissenberg, C.J., Zagorevski, A., van Breemen, O., and Jenner, G.A., 2007, The Notre Dame arc and the Taconic Orogeny in Newfoundland, *in* Hatcher, R.D., Jr., Carlson, M.P., McBride, J.H., and Martínez Catalán, J.R., *eds.*, 4-D framework of continental crust: Geological Society of America Memoir 200, p. 511–552.

van Staal, C.R., Castonguay, S., McNicoll, V., Brem, A., Hibbard, J., Skulski, T., and Joyce, N., 2009a, Taconic arc-continent collision confirmed in the Newfoundland Appalachians: Geological Society of America, 44th Annual Meeting, NE-section, p. 4.

van Staal, C.R., Whalen, J.B., Valverde-Vaquero, P., Zagorevski, A., and Rogers, N., 2009b, Pre-Carboniferous, episodic accretion-related, orogenesis along the Laurentian margin of the northern Appalachians, *in* Murphy, J.B., Keppie, J.D., and Hynes, A.J., *eds.*, Ancient orogens and modern analogues: Geological Society London Special Publications 327, p. 271–316.

Waldron, J.W.F., and van Staal, C.R., 2001, Taconian orogeny and the accretion of the Dashwoods block: A peri-Laurentian microcontinent in the Iapetus Ocean: Geology, v. 29, p. 811–814, http://dx.doi.org/10.1130/0091-7613(2001)029<0811:TOATAO>2.0.CO;2.

Weinberg, R.F., Regenauer-Lieb, K., and Rosenbaum, G., 2007, Mantle detachment faults and the breakup of cold continental lithosphere: Geology, v. 35, p. 1035–1038, http://dx.doi.org/10.1130/G23918A.1.

Whalen, J.B., Jenner, G.A., Longstaffe, F.J., Gariepy, C., and Fryer, B.J., 1997, Implications of granitoid geochemical and isotopic (Nd, O, Pb) data from the Cambrian-Ordovician Notre Dame Arc for the evolution of the central mobile belt, Newfoundland Appalachians: Geological Society of America Memoir, v. 191, p. 367–395.

Wiedenbeck, M., Allé, P., Corfu, F., Griffin, W.L., Meier, M., Oberli, F., Von Quadt, A., Roddick, J.C., and Spiegel, W., 1995, Three natural zircon standards for U–Th–Pb, Lu–Hf, trace element and REE analyses: Geostandards Newsletter, v. 19, p. 1–23, http://dx.doi.org/10.1111/j.1751-908X.1995.tb00147.x.

Williams, H., 1977, Ophiolitic mélange and its significance in the Fleur de Lys Supergroup, northern Appalachians: Canadian Journal of Earth Sciences, v. 14, p. 987–1003, http://dx.doi.org/10.1139/e77-091.

Williams, H., and Hiscott, R.N., 1987, Definition of the Iapetus rift-drift transition in western Newfoundland: Geology, v. 15, p. 1044–1047, http://dx.doi.org/10.1130/0091-7613(1987)15<1044:DOTLRT>2.0.CO;2.

Willner, A.P., Massonne, H., van Staal, C.R., and Zagorevski, A., 2012, Contrasting PT-evolution during an Ordovician arc-continent collision at the Laurentian margin in western Newfoundland (abstract): Geological Association of Canada – Mineralogical Association of Canada, Joint Annual Meeting, St. John's 2012, Program with Abstracts, p.152.

Winchester, J.A., Williams, H., Max, M.D., and van Staal, C.R., 1992, Does the Birchy Complex of Newfoundland extend into Ireland?: Journal of the Geological Society, v. 149, p. 159–162, http://dx.doi.org/10.1144/gsjgs.149.2.0159.

Yamasaki, T., and Gernigon, L., 2010, Redistribution of the lithosphere deformation by the emplacement of underplated mafic bodies: Implications for microcontinent formation: Journal of the Geological Society, v. 167, p. 961–971, http://dx.doi.org/10.1144/0016-76492010-027.

Zagorevski, A., Rogers, N., van Staal, C.R., McNicoll, V., Lissenberg, C.J., and Valverde-Vaquero, P., 2006, Lower to Middle Ordovician evolution of peri-Laurentian arc and back-arc complexes in Iapetus: Constraints from the Annieopsquotch accretionary tract, central Newfoundland: Geological Society of America Bulletin, v. 118, p. 324–342, http://dx.doi.org/10.1130/B25775.1.

Zagorevski, A., and van Staal, C.R., 2011, The record of Ordovician arc-arc and arc-continent collisions in the Canadian Appalachians during the closure of Iapetus –Chapter 12, *in* Brown, D., and Ryan, P.D., *eds.*, Arc-Continent Collision, Frontiers in Earth Sciences: Springer Verlag, Berlin Heidelberg, p. 341–371, http://dx.doi.org/10.1007/978-3-540-88558-0_12.

Received December 2012
Accepted as revised March 2013